Icarus 283 (2017) 326–342

Contents lists available at ScienceDirect

Icarus

journal homepage: www.elsevier.com/locate/icarus

Effects of varying environmental conditions on emissivity spectra of bulk lunar soils: Application to Diviner thermal infrared observations of the Moon

K.L. Donaldson Hanna[a,b,*], B.T. Greenhagen[c], W.R. Patterson III[a], C.M. Pieters[a], J.F. Mustard[a], N.E. Bowles[b], D.A. Paige[d], T.D. Glotch[e], C. Thompson[f]

[a] Department of Earth, Environmental and Planetary Sciences, Brown University, Providence, RI, USA
[b] Atmospheric, Oceanic and Planetary Physics, University of Oxford, Oxford, UK
[c] Applied Physics Laboratory, Johns Hopkins University, Laurel, MD, USA
[d] Department of Earth, Planetary, and Space Sciences, University of California Los Angeles, Los Angeles, CA, USA
[e] Department of Geosciences, Stony Brook University, Stony Brook, NY, USA
[f] ATK Mission Research, Logan, UT, USA

ARTICLE INFO

Article history:
Received 30 June 2015
Revised 18 May 2016
Accepted 19 May 2016
Available online 30 May 2016

Keywords:
Moon
Infrared observations
Spectroscopy
Regoliths
Experimental techniques

ABSTRACT

Currently, few thermal infrared measurements exist of fine particulate (<63 μm) analogue samples (e.g. minerals, mineral mixtures, rocks, meteorites, and lunar soils) measured under simulated lunar conditions. Such measurements are fundamental for interpreting thermal infrared (TIR) observations by the Diviner Lunar Radiometer Experiment (Diviner) onboard NASA's Lunar Reconnaissance Orbiter as well as future TIR observations of the Moon and other airless bodies. In this work, we present thermal infrared emissivity measurements of a suite of well-characterized Apollo lunar soils and a fine particulate (<25 μm) San Carlos olivine sample as we systematically vary parameters that control the near-surface environment in our vacuum chamber (atmospheric pressure, incident solar-like radiation, and sample cup temperature). The atmospheric pressure is varied between ambient (1000 mbar) and vacuum ($<10^{-3}$ mbar) pressures, the incident solar-like radiation is varied between 52 and 146 mW/cm^2, and the sample cup temperature is varied between 325 and 405 K. Spectral changes are characterized as each parameter is varied, which highlight the sensitivity of thermal infrared emissivity spectra to the atmospheric pressure and the incident solar-like radiation. Finally spectral measurements of Apollo 15 and 16 bulk lunar soils are compared with Diviner thermal infrared observations of the Apollo 15 and 16 sampling sites. This comparison allows us to constrain the temperature and pressure conditions that best simulate the near-surface environment of the Moon for future laboratory measurements and to better interpret lunar surface compositions as observed by Diviner.

1. Introduction

Apollo mare and highland soils (e.g. Pieters et al., 1993, 2000, 2006; Noble et al., 2001, 2006; Taylor et al., 2001, 2010) as well as basaltic rocks (Isaacson et al., 2011) and breccias (Noble et al., 2005) have been well-characterized across the visible- to near-infrared (VNIR) wavelengths to constrain the effects of mineralogy, mineral chemistries, ilmenite content, particle size and space weathering on their spectra. These laboratory analyses provided ground truth for remote sensing observations from Earth-based telescopic observations and spacecraft observations like those from National Aeronautics and Space Administration's (NASA) Clementine, Galileo and Lunar Prospector, European Space Agency's (ESA) Small Missions for Advanced Research in Technology (SMART-1), Japan Aerospace Exploration Agency's (JAXA) SELENE Kaguya, and Indian Space Research Organisation's (ISRO) Chandrayaan-1 as well as key insights into the composition and evolution of the lunar surface. Recently the Diviner Lunar Radiometer Experiment (Diviner), a nine band thermal infrared (TIR) radiometer, was launched onboard NASA's Lunar Reconnaissance Orbiter (LRO) (Paige et al., 2010a), making it necessary for detailed laboratory analysis of lunar samples across TIR wavelengths. Thermal infrared characterization will (1) aid in 'ground-truthing' the bulk thermal properties of the lunar surface (e.g. Bandfield et al., 2011, 2014; Vasavada et al. 2012; Ghent et al., 2014) and lunar surface compositions

* Corresponding author at: Atmospheric, Oceanic and Planetary Physics, University of Oxford, Oxford, UK Tel: +44 01865272089.
E-mail address: Kerri.DonaldsonHanna@physics.ox.ac.uk (K.L. Donaldson Hanna).

http://dx.doi.org/10.1016/j.icarus.2016.05.034
0019-1035/

(e.g. Greenhagen et al., 2010; Glotch et al., 2010, 2011; Allen et al., 2012; Donaldson Hanna et al., 2012a, 2015a), (2) estimate the spectral effects due to space weathering (e.g. Glotch et al. 2015; Lucey et al., 2016), (3) better constrain the near surface (upper hundreds of microns) environmental conditions of the Moon (e.g. Thomas et al., 2012; Donaldson Hanna et al., 2012b), and (4) support thermal models of the surface (upper meter), in particular the semi-permanently and permanently shadowed regions at the lunar poles (e.g. Paige et al., 2010b; Foote et al., 2012; Johnson et al., 2013; Warren et al., 2014; Greenhagen et al., 2015).

The fine particulate nature of the regolith and the lack of an appreciable atmosphere complicate the interpretation of thermal infrared emission observations of airless bodies like the Moon and asteroids. On the Moon and other airless bodies there are no interstitial atmospheric gases between regolith grains to transfer heat through conduction; rather heat is transferred through radiation and grain-to-grain contacts. Radiative cooling becomes very efficient at the near-surface (upper hundreds of microns) as it is exposed to the coldness of space, thus setting up a strong thermal gradient between the near-surface and the portions of the upper centimeter of regolith being heated by incident solar radiation (e.g. Logan and Hunt, 1970; Logan et al., 1973; Henderson and Jakosky, 1994). This is unlike planets with atmospheres like the Earth and Mars where the pore space between regolith grains is filled with interstitial gases, which allows heat to transfer efficiently from depth to the surface through conduction. Thus, the upper hundreds of microns of regolith on planets with an atmosphere are nearly isothermal (e.g. Henderson and Jakosky, 1994).

The depth in the lunar regolith from which the measured emission originates depends on the wavelength as well as the composition and physical nature of the regolith materials. As the wavelength varies so does the depth from which the measured thermal emission originates, thus different temperatures are measured owing to the thermal gradient in the near-surface (Logan and Hunt, 1970; Logan et al., 1973; Henderson and Jakosky, 1994, 1997). Across wavelength regions where materials have high absorption coefficients and surface scattering dominates (spectral regions covering the reststrahlen bands) the measured emission comes from the cooler surface (upper tens of microns). Across transparent regions of the spectrum where materials have low absorption coefficients and volume scattering dominates (spectral regions covering the Christiansen feature and transparency feature) the measured emission comes from deeper (upper hundreds of microns), warmer portions of the near-surface. Therefore, a single thermal infrared emission measurement of the lunar surface from orbit is sampling multiple depths and temperatures within the upper hundreds of microns and cannot easily be reconciled with a single Planck function (Logan and Hunt, 1970; Logan et al., 1973; Henderson and Jakosky, 1994, 1997). Thus, thermal infrared spectral measurements represent an effective emissivity of the lunar surface as they include diagnostic features due to composition and particle size that are affected by the thermal gradient.

Previous laboratory emissivity measurements of particulate rocks, minerals, and lunar soils under vacuum and lunar-like conditions (Hunt and Salisbury, 1964; Murcray, 1965; Logan and Hunt, 1970; Logan et al., 1973; Salisbury and Walter, 1989; Henderson et al., 1996; Thomas et al., 2012; Donaldson Hanna et al., 2012a, 2012b, 2015a) observed an enhancement in the spectral contrast of the Christiansen feature (CF) and a shift in the CF position to shorter wavelengths (higher wavenumbers) when compared to spectra measured under isothermal or 'Earth-like' conditions. These observed spectral differences were attributed to the strong thermal gradient generated within the uppermost portion of particulate samples from the vacuum environment and solar-like incident radiation (Logan et al., 1973; Henderson et al., 1996; Henderson and Jakosky, 1997). The observed spectral changes under vacuum and lunar-like environmental conditions demonstrate the need for making laboratory measurements under comparable near-surface conditions for the interpretation of remote sensing observations of airless bodies like the Moon, Mercury, Mars' moons Phobos and Deimos, and asteroids.

Currently, few measurements have been published of fine particulate (<63 μm) samples (e.g. minerals, mineral mixtures, rocks, meteorites, and lunar soils) measured under simulated lunar conditions. These laboratory spectral measurements are fundamental for interpreting thermal infrared observations by Diviner and future TIR lunar observations. In this work, we make thermal infrared spectral measurements of a suite of well-characterized Apollo bulk lunar soils as we systematically vary parameters that control the near-surface environment in our vacuum environment chamber (atmospheric pressure, incident solar-like radiation, and sample cup temperature). The observed spectral changes are characterized as each parameter is varied to constrain which parameters have the largest effect on the spectral measurements. Finally spectral measurements of Apollo 15 and 16 bulk lunar soils are compared with Diviner TIR observations of the Apollo 15 and 16 sampling sites. This comparison allows us to constrain the temperature and pressure conditions that best simulate the near-surface environment of the Moon for future laboratory measurements and to better interpret lunar surface compositions as observed by Diviner.

2. Background

Remote sensing observations provide key insights into the formation and evolution of a planet's surface through the determination of its surface composition. A fundamentally important component to interpreting the composition of a planet's surface is a suite of laboratory measurements of well-characterized analogue materials. Laboratory thermal infrared spectral measurements of analogue samples have been successfully applied to map planetary compositions on Earth and Mars (e.g.; Ramsey and Christensen, 1998; Feeley and Christensen, 1999; Hamilton and Christensen, 2000; Wyatt et al., 2001; Rogers et al., 2007). TIR emissivity spectra are sensitive to the chemistry and structure of all common rock-forming silicates and exhibit unique spectral features that can be used to identify them. These diagnostic features include the Christiansen feature (CF), reststrahlen bands (RB), and transparency features (TF) as seen in Fig. 1. The CF is an emissivity maximum resulting from a rapid change in a material's refractive index at wavelengths shorter than those of the fundamental molecular vibration bands. Conel (1969) found that the CF position in silicates is diagnostic of bulk mineralogy as it changes with the change in bond strength and molecular geometry associated with changing mineralogy. As seen in Fig. 1, plagioclase feldspars (which have little Fe, but high Al and Ca contents) have shorter wavelength CF positions than pyroxenes and olivines (which have high Fe and/or Mg content and low Al). The RB are the fundamental molecular vibration bands due to stretching (Si–O–Si, Si–O–Al, Si–Si, and Si–Al) and bending motions (O–Si–O and O–Al–O). The fundamental vibration bands occur in spectral regions where surface scattering dominates (regions where minerals have high absorption coefficients) for particle sizes and packing states of typical regoliths. The exact frequencies, shapes and intensities, and number of absorptions in the RBs are dependent on atomic masses and bond lengths, geometry, and bond strengths within mineral crystal lattices. Because all minerals consist of unique structures and/or compositions, virtually every mineral has a different set of vibrational characteristics and thus a highly diagnostic set of RB absorptions (e.g. Lyon, 1964; Conel, 1969; Salisbury and Walter, 1989; Hamilton, 2000). The TF is an emissivity minimum caused by volume scattering of fine particulates (typically < 63 μm) in a

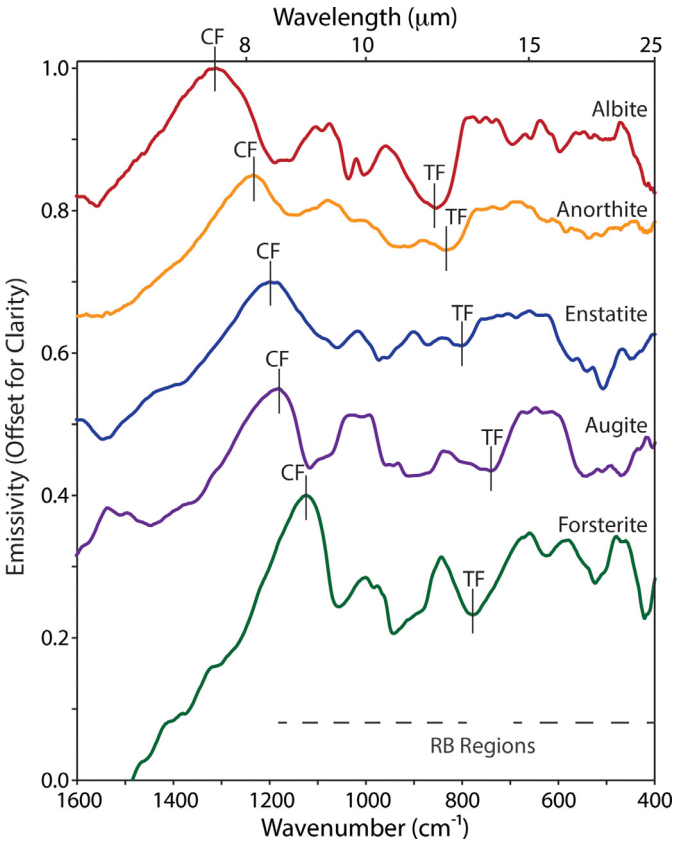

Fig. 1. Full resolution laboratory spectra of fine particulate (<25 μm) silicate minerals measured under ambient conditions (samples were heated from below to ~350 K and atmospheric pressure inside the chamber was held at ~1000 mbar). Thermal infrared diagnostic features are labeled as follows: CF (Christiansen feature), RB (reststrahlen bands), and TF (transparency feature). Spectra are normalized to 1.0 at peak emission and offset by 0.15 emissivity from one another for clarity. Figure is adapted from Donaldson Hanna et al. (2012b) Mineral chemistries of each of the silicate minerals are provided in Donaldson Hanna et al. (2012b).

spectral region of relative transparency between the principal RB. TFs, like the CF, are indicators of composition and particulate size; generally, as particle size decreases, the spectral contrast of the TFs increases due to volume scattering (e.g. Salisbury and Walter, 1989; Cooper et al., 2002).

3. Experimental set-up

The Asteroid and Lunar Environment Chamber (ALEC) is a vacuum chamber that resides in Brown University's Reflectance Experiment Laboratory (RELAB). ALEC was built by ATK Mission Research to simulate the space environment experienced by the near-surface regolith of airless bodies such as the Moon and asteroids. The lunar environment is simulated for particulate sample materials placed inside the chamber by (1) removing atmospheric gases inside the chamber to a pressure $< 10^{-4}$ mbar, which is sufficient to simulate lunar heat transport processes within the sample (e.g. Logan et al., 1973), (2) cooling the chamber to simulate the cold space environment into which the lunar surface radiates heat (85 K), and (3) heating the sample material from above and below to simulate the incident solar radiation on the Moon's surface and the ambient temperature of the Moon at depth within the regolith.

Images of ALEC in Fig. 2 show the general experimental set-up. To control the atmospheric pressure inside the chamber, a Pfeiffer turbo-molecular pump is attached to one of ALEC's flanges (seen in Fig. 2A). The chamber can be pumped down to pressures $< 10^{-3}$ mbar when the interior of the chamber is at room temperature and $< 10^{-4}$ mbar when ALEC is cryopumped. For experiments with ambient to low atmospheric pressure (e.g. Earth- and Mars-like pressures), dry air (<5 ppm H_2O) is used to backfill the environment chamber to any desired pressure ≤1000 mbar using a Pfeiffer wide range gauge and Pirani measurement system. The environment chamber is cooled by liquid nitrogen (LN_2) running through a network of cooling lines attached to the bottom of the sample stage. A stable thermal environment is created using an aluminum radiation shield (Fig. 2C) that sits on top of the sample stage. As seen in Fig. 2D, each sample cup is surrounded by a radiation shroud that is painted with black, high emissivity paint to create a cold, low-emission environment for heated samples to radiate into. To ensure that the thermal environment inside the chamber is stable and as homogeneous as possible, spectral measurements are not made until temperatures from temperature sensors on two different places on the sample stage and a temperature sensor standing off of the sample stage at a height of the sample cup all measure 85 ± 0.5 K.

The solar irradiance on the lunar surface is simulated by heating sample materials from below using heaters embedded in the base of thermally isolated sample cups and from above using a 200 W quartz-halogen lamp heat source (Fig. 2B). A fused silica window sits between the quartz-halogen lamp and the sample cup to reduce (a) the contribution of reflected radiation to the measured spectrum and (b) long wave radiation heating the sample. Initial tests of the quartz-halogen lamp demonstrated that when the lamp was turned on between 30 and 100% of the lamp wattage, the irradiance measured at the height of the sample cup was between 3 and 146 mW/cm^2; thus when the lamp is turned on at 90 to 100% of the lamp wattage the irradiance on the sample is similar to the total solar irradiance measured at the top of the Earth's atmosphere (136.6 mW/cm^2) (Fröhlich, 2006). A detailed diagram of the environment surrounding each sample cup as well as the heating configuration is illustrated in Fig. 3.

Spectral measurements were made using RELAB's Thermo Nicolet Nexus 870 Fourier Transform Infrared (FTIR) spectrometer. ALEC is connected to the FTIR spectrometer through a potassium bromide (KBr) emission port window and an aluminum shroud purged with dry air (as seen in Fig. 2A). The Thermo Nicolet's KBr beam splitter and deuterated triglycine sulfate (DTGS) detector allow laboratory spectra to be collected at a resolution of 4 cm^{-1} over a nominal 5–25 μm (400–2000 cm^{-1}) spectral range. The wavenumber precision of the Thermo Nicolet Nexus 870 FTIR is <0.01 cm^{-1} at 2000 cm^{-1} owing to the accuracy of the scanning mirror position (2 nm). The spectrometer is purged with dry air (< 5 ppm H_2O) for instrument stability and to remove any particulates, water vapor, and CO_2.

For spectral measurements, 500 interferograms are collected and averaged by the instrument to provide the signal-to-noise ratio required to detect features with spectral contrast on the order of 1%. To demonstrate the stability of the FTIR over the 500 interferogram collection time, five measurements of 100 interferograms each were made of San Carlos olivine (particle sizes <25 μm) under ambient or Earth-like conditions. The average and standard deviation of those five measurements along with the repeat measurements are shown in Fig. 4. The standard deviation of the repeat measurements is less than 0.1% across the ~7.1–15.4 μm (1400–650 cm^{-1}) spectral range and less than 1.6% across the ~15.4–25.0 μm (650–400 cm^{-1}) spectral range. The calibration of spectral measurements of sample materials is achieved by making regular measurements of a blackbody target at two temperatures (375 and 405 K) also with 500 multiple interferograms (Ruff et al., 1997; Thomas et al., 2012) and accounting for the spectral shape of the blackbody target. The blackbody target used in this analysis is particulate blast furnace slag obtained from the Planetary Emissivity Laboratory (PEL) of the German Aerospace Center (DLR)

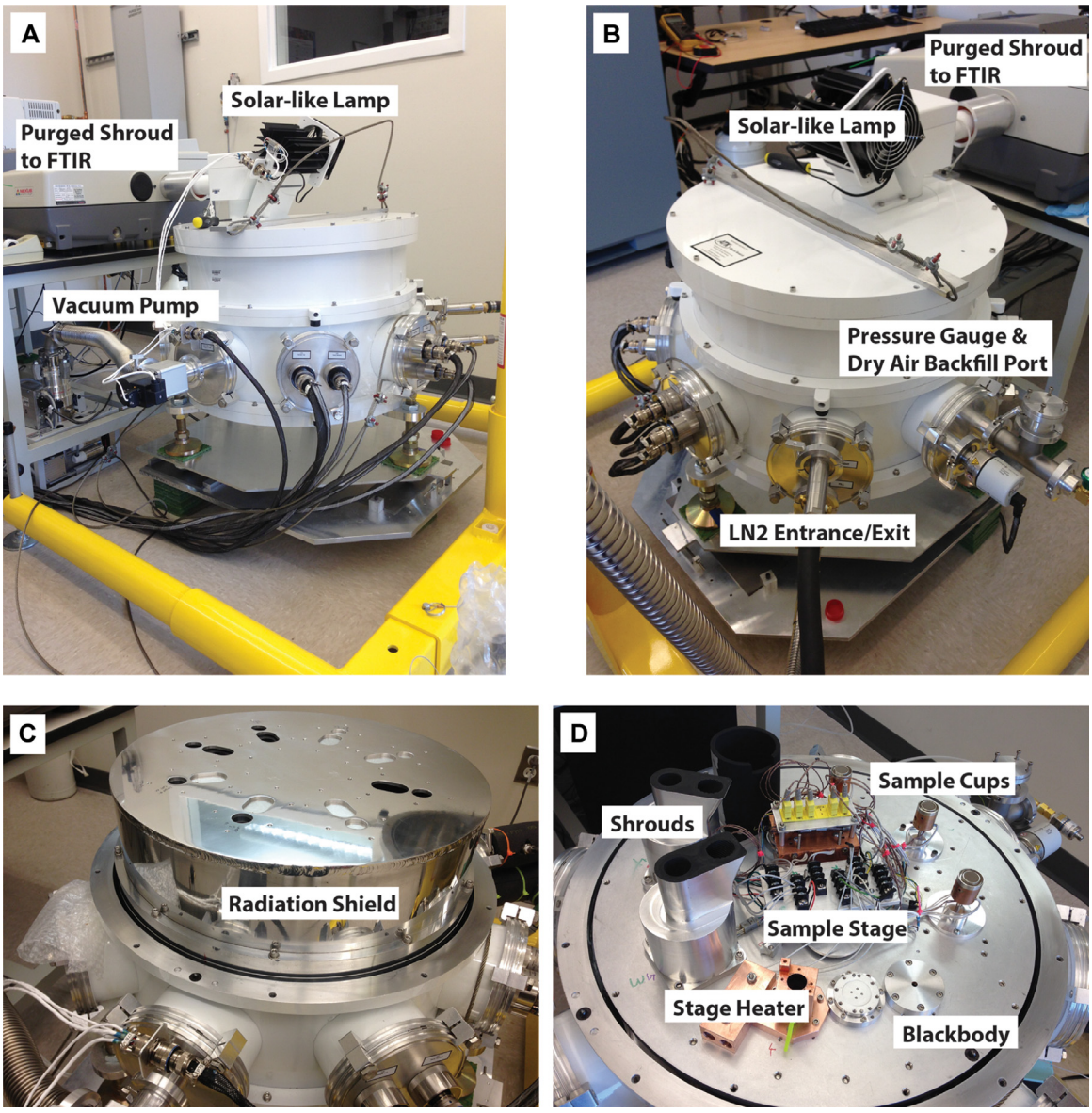

Fig. 2. General configuration of the environment chamber. (A) ALEC is connected to a Thermo Nicolet Nexus 870 FTIR spectrometer using a shroud purged with dry air. The chamber is pumped to vacuum pressures using the attached Pffeifer turbo-molecular pump. (B) The chamber can be backfilled to any pressure with dry air and cooled with LN_2. Samples are heated from above using the solar-like lamp. (C) A radiation shield sits on top of the sample stage, which cools the environment surrounding the sample cups. (D) Six sample cups sit on a rotating sample stage and are enclosed in shrouds. Samples are heated from below using heaters on the base of the sample cups. Two sensors sit on the sample stage and one is attached to the base of a non-heated sample cup to monitor the interior temperature of the chamber.

in Berlin (Maturilli et al., 2013). The slag was chosen because it (1) has a very high emissivity, (2) has a nearly flat emissivity spectrum across the 5–25 μm spectral region (see Fig. 5), and (3) does not outgas when heated in a vacuum above 700 K. In addition, an advantage of using a particulate blackbody material (63–125 μm) is that it can be measured in the same sample cup and under the same conditions as any of the sample materials.

4. Samples and methods

4.1. Apollo bulk lunar soils

Lunar soils measured in this initial study include Apollo samples requested from NASA's Curation and Analysis Planning Team for Extraterrestrial Materials (CAPTEM) as a part of the Thermal Infrared Emission Studies of Lunar Surface Compositions Consortium (TIRES-LSCC). The consortium includes four research institutions (Brown University, the University of Oxford, Johns Hopkins University Applied Physics Laboratory, and Stony Brook University) and was formed to characterize bulk lunar soils across thermal infrared wavelengths. In particular, these laboratory measurements will provide better context for TIR spectral effects due to variable soil composition and maturity as well as aiding in the interpretation of Diviner observations (e.g. Paige et al., 2010a; Greenhagen et al., 2010, 2012; Glotch et al., 2010, 2011, 2015; Allen et al., 2012; Song et al., 2013; Donaldson Hanna et al., 2014) and future thermal infrared data sets of airless bodies.

We focus on surface samples that were collected as comprehensive or reference samples from sampling stations at the Apollo 11, 14, 15, 16, and 17 landing sites. Samples collected as comprehensive or reference soils for a landing site are assumed to be the most relevant to Diviner orbital observations for that sampling station. This initial study was also limited to soil samples whose composition and particle size distribution were previously

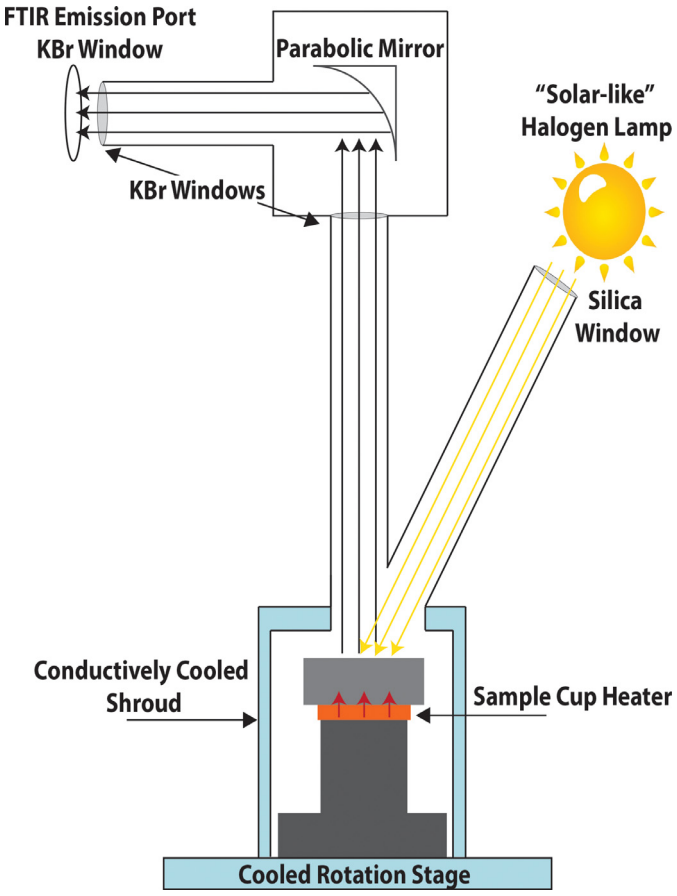

Fig. 3. Diagram of a sample cup in ALEC illustrating its surrounding environment. Each sample cup sitting on the rotation stage is covered by a shroud that is cooled conductively from the stage. The sample can be heated from above using the solar-like halogen lamp and/or from below using the heater at the base of the cup. The sample's emitted radiation hits a collimating parabolic mirror before exiting ALEC through a potassium bromide (KBr) window into the emission port of the Thermo Nicolet Nexus 870 FTIR.

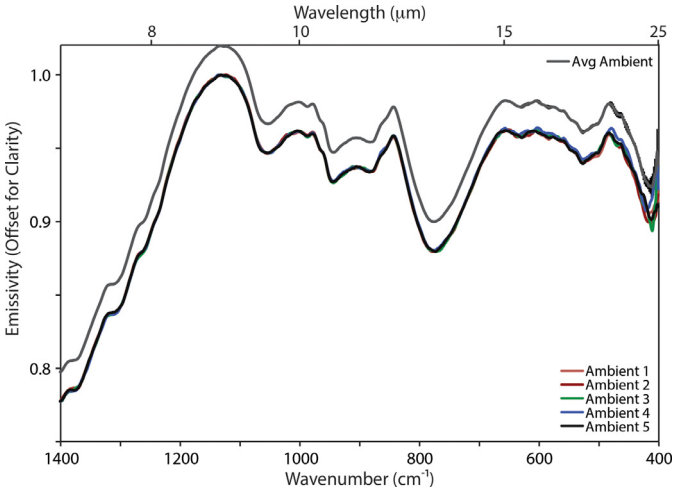

Fig. 4. Ambient ('Earth-like') spectra of San Carlos olivine (< 25 μm) measured in ALEC. Five repeat ambient measurements were made with 100 interferograms each. The average ambient spectrum includes those five repeat measurements and demonstrates the stability of the FTIR spectrometer over a 500 interferogram collection time. The standard deviation (1σ) of the repeat measurements is included as black error bars on the average spectrum. The ambient spectrum is offset from the repeat ambient spectra by 0.02 for clarity.

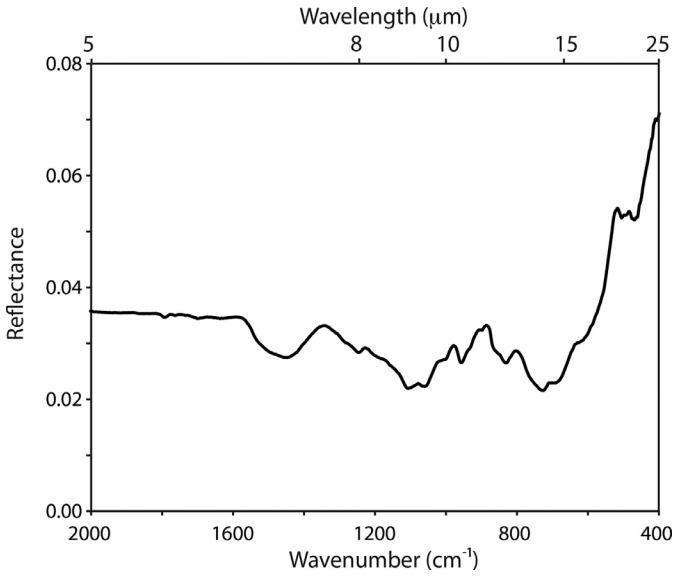

Fig. 5. Reflectance spectrum of the blast furnace slag particulate sample (63–125 μm) used in the blackbody calibration. The blast furnace slag material has a high emissivity and its spectrum is nearly flat across the 5–25 μm spectral region. The average variance in reflectance across the spectrum is 2% with the largest departure at ~5% near 25 μm.

well characterized and have at least 3.5 g available for analysis (as required by the size of sample cups in ALEC and other environment chambers). Our suite of <1 mm sieved lunar soils includes 10084, 14259, 15071, 15201, 15411, 66031, 67701, 70181, 72501, and 79221. Sub-split numbers for each of the Apollo samples are provided in Table 1. The curatorial laboratory prescreened these lunar soil samples with a dry sieve and no additional sieving or particle size sorting was done to the < 1 mm soil samples for our work. The suite of soils includes Apollo samples of varying composition and varying maturity, where the maturity of the lunar samples is expressed as I_s/FeO (the intensity of the characteristic ferromagnetic resonance of a lunar soil normalized to its total iron content (Morris 1976, 1978)) and its value increases as a function of exposure time on the lunar surface. Detailed modal analyses, maturities, and mineral chemistries are provided in Tables 2–4.

4.1.1. Sample preparation for spectral measurements

For terrestrial mineral samples like the San Carlos olivine sample (Figs. 4 and 6), where the amount of sample is not limited to 3.5 g, sample material is carefully spooned into a stainless steel ALEC sample cup. The sample cup is overfilled with sample material and a flat edge is taken across the sample to 'flatten' its surface. However, the ALEC sample cup is sufficiently large (40 mm in diameter and 2 mm deep) that the requested 3.5 g of lunar soil sample material does not overfill the sample cup, so the surface cannot be flattened with a flat edge. Instead each of the Apollo soil samples is carefully spooned into the stainless steel ALEC sample cup and the cup is gently tapped five times to break up any sample packing from the spoon and to "flatten" the surface while limiting any particle size sorting due to over tapping the sample.

The tapping method for 'flattening' the sample's surface is not as repeatable and does not produce as flat of a surface as taking a flat edge across it. Using the tapping method on the Apollo samples will also subtly vary the porosity or packing between samples, which can affect the spectral contrast in the reststrahlen bands and transparency feature (Salisbury and Wald, 1992; Donaldson Hanna et al., 2015b). Donaldson Hanna et al. (2015b) measured Apollo sample 15071 under simulated lunar conditions using the Simulated Lunar Environment Chamber at the University of Oxford

Table 1
Lunar soil sample numbers and sub-split numbers.

Sample number	10084	14259	15201	15411	66031	67701	72501	79221
Sub-split number	1854	83 91	330	24 25 26 49	67	219	81	153

Table 2
Particle size fractions and maturities of bulk lunar soils.

Sample #	10084[a]			14259[b]			15071[b]	15201[b]	15411[b]	66031[b]	67701[b]		70181[b]	72501[b]				79221[b]	
Sub-split #	8	166	167	52	64	88	19	17	42	2	16	17	1	1	15	26	29	1	27
Avg Particle Size (μm)	52.2	69.4	63.4	67.9	73.8	48.4	78.6	60.4	97.4	120.7	161.5	135.8	62.1	66.1	71.8	89.6	65.4	89.6	92.8
Std Dev Particle Size (μm)	260.6	267.9	246.6	262.4	220.7	188.2	181.8	211.7	115.8	186.9	167.2	153.9	216.1	201.7	189.5	220.7	225.3	150.7	129.4
Percent < 75 μm	60.5	51.6	52.8	53.8	46.7	60.1	45.3	56.1	45.7	40.7	34.0	32.7	53.4	54.5	55.2	47.0	55.7	53.2	40.0
I_s/FeO[c]	78	78	78	85	85	85	52	68	43	102	39	39	47	81	81	81	81	81	81

[a] King et al. (1971).
[b] Graf (1993).
[c] Morris (1978).

Table 3
Modal content of bulk lunar soils.

	10084[a]	14259[b]	15071[c]	15201[d]	15411[d]	66031[e]	67701[e]	70181[f]	72501[a]	79221[f]
Agglutinates	52.0	51.7	39.2					56.0	37.6	44.4
Basalt		1.0	5.6					14.0		14.4
KREEP basalt			1.3							
Mare basalt	24.0								2.9	
Feldspathic basalt	1.1								0.2	
Breccia		25.3	7.5					7.5		10.5
Breccia, light	0.8								2.4	
Breccia, dark	7.5								22.6	
Poikilitic breccia									9.7	
Anorthosite			1.1					0.3		0.3
Norite										
Gabbro										
Anorthosite, Norite	0.4								5.2	
Plagioclase	1.9	4.7	9.2			54.0	74.0	4.3	10.9	6.9
Pyroxene		4.3	23.9			6.8	7.6	10.6		6.5
Olivine			1.9			5.9	4.1			
Ilmenite			0.8					2.3		1.3
Mafic Mineral	4.2								5.2	
Opaque	1.1								0.1	
Glass Other	6.6	12.8	6.5			33.4	14.3		3.0	11.5
Orange Glass								3.0		4.2

[a] Simon et al. (1981).
[b] McKay et al. (1972).
[c] Basu et al. (1981).
[d] No modal content available
[e] Taylor et al. (2012).
[f] Heiken and McKay (1974).

(Thomas et al., 2012) with varying packing styles (including tapping the sample and taking a flat edge across the surface). A comparison of emissivity spectra of Apollo 15071 when the surface has been tapped and when a flat edge has been taken across it demonstrates that (1) the CF, RB and TF are observed at the same wavelength positions and (2) the spectral contrast differences in the CF, RB and TF regions of the spectra are 0.8, 0.2 and 1.2%, respectively. In the present work, the spectral contrast differences due to porosity/packing variations are included as errors when calculating the spectral contrast of features and when full resolution laboratory spectra are re-sampled to Diviner's spectral bands.

4.2. Experimental conditions

An initial set of ALEC experiments were conducted to assess how systematic variations in the atmospheric pressure inside the chamber, irradiance from the solar-like halogen lamp, and heat from the sample cup affect thermal infrared spectral measurements of lunar regolith samples. Experimental conditions for the laboratory measurements are provided in Table 5 and were chosen to encompass a range of conditions on airless bodies like the Moon. Spectral changes due to systematic variations in the atmospheric pressure inside the chamber were tested under the following conditions (a) the atmospheric pressure was varied between 980 ± 20, 5 ± 2, and $< 10^{-3}$ mbar, (b) the sample was heated from below to 405 ± 0.2 K, (c) the solar-like halogen lamp was not turned on, and (d) the environment chamber was at room temperature (297 ± 2 K). Spectral differences due to systematic variations in the power of the halogen lamp were tested under the following conditions (a) the atmospheric pressure inside the chamber was held to $< 10^{-4}$ mbar, (b) the sample was heated from below to 405 ± 0.2 K, (c) the power of the solar-like halogen lamp was varied between 80 and 200W, which equates to irradiances between ~52 and 146 mW/cm^2, and (d) the environment

Table 4
Lunar soil chemistries.

	10084[a]	14259[b]	15071[c]	15201[d]	15411[e]	66031[f]	67701[g]	70181[h]	72501[i]	79221[i]
SiO_2	42.00	48.16	46.95	46.35	46.22		45.11	40.9	45.12	41.67
TiO_2	7.54	1.73	1.60	1.34	1.09		0.26	8.40	1.56	6.52
Al_2O_3	13.55	17.60	12.70	17.73	15.08	26.7	30.27	12.40	20.64	13.57
FeO	15.81	10.41	16.29	11.66	13.36	5.80	2.96	16.55	8.77	15.37
MnO	0.21	0.14	0.22	0.16	0.176	0.08	0.04	0.21	0.11	0.21
MgO	7.88	9.26	10.75	10.48	11.74	6.80	4.38	9.76	10.08	10.22
CaO	11.96	11.25	10.49	11.68	10.91	14.6	16.60	10.97	12.86	11.18
Na_2O	0.44	0.52	0.33	0.44	0.36	0.44	0.64	0.38	0.40	0.34
K_2O	0.14	0.50	0.09	0.19	0.16		0.06	0.09	0.16	0.09
P_2O_5	0.10		0.13	0.19	0.17		0.03	0.07	0.13	0.06
Total	99.63	99.57	99.55	100.22	99.27		100.35	99.73	99.83	99.23

[a] Korotev and Gillis (2001).
[b] Rose et al. (1972).
[c] Duncan et al. (1975).
[d] Cuttitta et al. (1973).
[e] Willis et al. (1972).
[f] Korotev (1982).
[g] Rose et al. (1975).
[h] Rose et al. (1974).
[i] Rhodes et al. (1974).

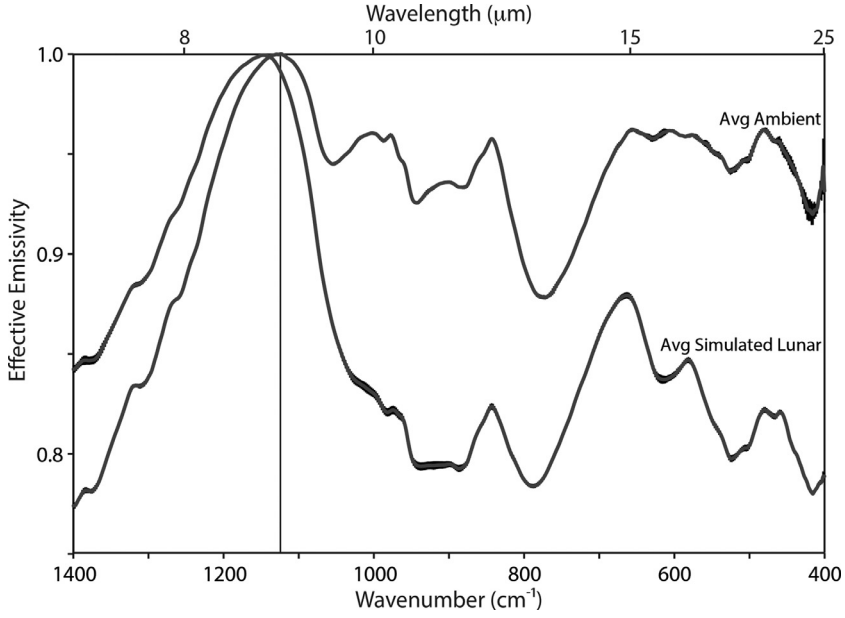

Fig. 6. Average ambient ('Earth-like') and simulated lunar (90% Lamp experimental conditions in Table 7) spectra of San Carlos olivine (<25 μm) measured in ALEC. Each average spectrum includes three repeat measurements made with 500 interferograms each. The standard deviations (1σ) of the repeat measurements are included as black error bars on the average spectra. The vertical line indicates the identified CF position of the ambient olivine spectrum (8.88 μm) and demonstrates the shift of the CF position under simulated lunar conditions.

Table 5
ALEC experimental conditions for lunar soil spectral measurements.

	Sample cup Temp (K)	Lamp power (W)	Irradiance on sample (mW/cm^2)	Chamber pressure (mbar)	Chamber temp (K)
Ambient(Earth-like)	405 ± 0.2			980 ± 20	297 ± 2
5 mbar (Mars-like)	405 ± 0.2			5 ± 0.2	297 ± 2
Vacuum	405 ± 0.2			$<10^{-3}$	297 ± 2
325 K	325 ± 0.2	160 ± 0.1	129 ± 2	$<10^{-4}$	85 ± 0.5
350 K	350 ± 0.2	160 ± 0.1	129 ± 2	$<10^{-4}$	85 ± 0.5
375 K	375 ± 0.2	160 ± 0.1	129 ± 2	$<10^{-4}$	85 ± 0.5
405 K*	405 ± 0.2	160 ± 0.1	129 ± 2	$<10^{-4}$	85 ± 0.5
70% Lamp	405 ± 0.2	80 ± 0.1	52 ± 2	$<10^{-4}$	85 ± 0.5
80% Lamp	405 ± 0.2	115 ± 0.1	71 ± 2	$<10^{-4}$	85 ± 0.5
90% Lamp*	405 ± 0.2	160 ± 0.1	129 ± 2	$<10^{-4}$	85 ± 0.5
100% Lamp	405 ± 0.2	200 ± 0.1	146 ± 2	$<10^{-4}$	85 ± 0.5

* 405 K and 90% Lamp experimental conditions are the same measurement conditions.
** Uncertainties in sample cup temperature, lamp power, chamber pressure, and chamber temperature are maximum uncertainties.

chamber was cooled to 85 ± 0.5 K. Variations in emissivity spectra due to the amount of heat being applied to the bottom of the sample were tested under the following conditions (a) the atmospheric pressure inside the chamber was held to $< 10^{-4}$ mbar, (b) the sample was heated from below to temperatures between 325 ± 0.2 K and 405 ± 0.2 K, (c) the power of the solar-like halogen lamp was held constant at 200 watts (irradiance on the sample ~129 mW/cm^2), and (d) the environment chamber was cooled to 85 ± 0.5 K.

Uncertainties in the sample cup temperature are maximum uncertainties and are related to the accuracy of the Lakeshore temperature controllers and heaters on the sample cups. Uncertainties in the atmospheric pressure at Earth- and Mars-like pressures are maximum uncertainties and are related to the accuracy in backfilling the chamber with dry air. Repeated spectral measurements made when the atmospheric pressure inside the environment chamber varies, but is $<10^{-3}$ show no differences due to changes in the atmospheric pressure. Thus, all pressures under vacuum and cooled conditions are reported as $< 10^{-3}$ mbar and $< 10^{-4}$ mbar, respectively. Under all experimental conditions the samples were allowed to come to equilibrium before spectral measurements were taken. The peak-to-peak signal of the FTIR interferogram is monitored and a sample is deemed to be in equilibrium once the signal has stopped changing. For ambient measurements, it takes approximately 10 minutes for samples to come to equilibrium once the sample heater achieves the set temperature. For simulated lunar environment (SLE) measurements, it takes approximately 15 minutes for samples to come to equilibrium once the solar-like halogen lamp is turned on. Three spectral measurements of San Carlos olivine (particle sizes < 25 μm) of 500 interferograms each were made under ambient and simulated lunar environment (100% Lamp in Table 5) conditions after samples reached equilibrium. Average ambient and SLE emissivity spectra in Fig. 6 demonstrate that once samples are at equilibrium the maximum standard deviation of the emissivity of multiple measurements across the entire spectral range is 1.4 and 0.3%, respectively. Pure mineral spectra are shown here to demonstrate the differences due to the thermal stability of the sample because Logan et al. (1973) and Henderson and Jakosky (1997) showed that pure minerals are more sensitive to differences in the environment under which they are measured than rocks. Thus, differences in the San Carlos olivine spectra due to the thermal stability of the sample should be an upper limit for differences in the lunar soil measurements.

4.3. Data analysis methods

Previous laboratory measurements made under lunar-like conditions observed shifts in the CF position and an increase in the spectral contrast between the CF and RB when compared to measurements made under Earth-like conditions (e.g. Logan et al., 1973; Salisbury and Walter, 1989; Henderson et al., 1996; Donaldson Hanna et al., 2012a, 2012b; Thomas et al., 2012). As these features are demonstrated to be the most sensitive to the environmental conditions, we will use the same metrics for assessing our thermal infrared emissivity spectra of the lunar soil samples. These metrics, the wavelength position of the CF and the spectral contrast between the CF and the RB, are provided in Table 6. The wavelength position (μm) of the CF was identified in each lunar soil spectrum by fitting a third degree polynomial to a portion of the 7–9 μm (~1100–1400 cm^{-1}) spectral range. The wavelength of the maximum emissivity in the polynomial fit was identified as the wavelength position of the CF. In order to best fit the emissivity value and shape of the CF, the wavelength range was varied for each spectrum. Due to the non-unique nature of identifying the CF position using this approach, the maximum difference in the CF position is ±0.02 μm as the spectral range is changed. Similar methods were used previously to identify the CF position for a range of plagioclase feldspar samples measured under varying environmental conditions (Donaldson Hanna et al., 2012a). The spectral contrast between the CF and the RB for each lunar soil is calculated by taking the emissivity value at the CF wavelength position, which is assumed to be 1 at the CF, subtracting the emissivity value at the RB identified near 10.5 μm, and multiplying by 100. The RB near 10.5 μm was chosen for this analysis, as it is the most apparent RB feature in all of the lunar soils under all of the environmental conditions, therefore it is best for illustrating the change in spectral contrast as the environmental conditions change. Uncertainties associated with the estimation of the spectral contrast include sample porosity (maximum of 0.2% under SLE conditions) and the thermal stability of the sample during measurement (maximum of 0.3% under SLE conditions) as discussed earlier in the manuscript. As these uncertainties are unrelated they have been summed in quadrature.

To estimate how the temperature of the sample varies with environmental condition the brightness temperature was calculated and provided in Table 6. The brightness temperature is calculated as a function of wavelength assuming the maximum brightness temperature is at the wavelength position of the CF, where we have assumed emissivity is 1 (similar to the approach of Ruff et al. 1997). Also, when calculating the brightness temperature an assumption is made that the sample is in thermal equilibrium with its surroundings, which we know not to be the case for measurements made under simulated lunar conditions. Thus, for measurements made under SLE conditions the calculated brightness temperatures are just estimates. Uncertainties in the estimated brightness temperatures can arise from the thermal stability of the sample. Analyses of repeat measurements of San Carlos olivine under ambient and SLE conditions show that the maximum difference in brightness temperatures are 0.1 K and 1.5 K, respectively. We use the estimated brightness temperatures as rough guides for understanding how the sample temperatures compare with Diviner observations of the Apollo sampling stations.

Spectra of Apollo 15 and 16 bulk soils measured under varying environmental conditions are compared to Diviner thermal infrared observations of the Apollo sampling stations at which the bulk lunar soils were collected. For this comparison, full resolution laboratory emissivity spectra were re-sampled to Diviner's three "8 μm" spectral bands (bands 3, 4, and 5 with center wavelengths at 7.81, 8.28 and 8.55 μm), using the band pass filters for each spectral band (Paige et al., 2010a). Each laboratory spectral measurement was multiplied by the transmission per wavelength of each "8 μm" filter and then averaged across the wavelength range of each "8 μm" filter. Uncertainties in the re-sampled laboratory spectra are dominated by the uncertainties associated with the thermal stability of the sample as discussed earlier in the manuscript. The maximum difference in emissivity values for Diviner bands 3, 4, and 5, are 0.05, 0.09, and 0.1%, respectively. Diviner radiance data of the Apollo landing sites have been limited to lunar midday (10:00 to 14:00 local time) and emission angles <5°. Radiance data are binned and averaged at 128 pixels per degree and then converted to three point emissivity spectra as described by Greenhagen et al. (2010). Diviner emissivity values are then corrected for local lunar time, latitude and topography to account for the effects of anisothermality (Greenhagen et al., 2011).

5. Results

Spectral measurements of the suite of well-characterized lunar soil samples made under ambient and simulated lunar (Ambient and 90%Lamp experimental conditions in Table 5) conditions are plotted in Fig. 7. Spectral measurements made under the remaining experimental conditions in Table 5 (5 mbar, Vacuum,

Table 6
Lunar soil CF positions (μm), spectral contrast (%) and brightness temperatures (K).

CF Positions (μm) Max Uncertainty ± 0.02 μm	1000 mbar	5 mbar	$\leq 10^{-3}$ mbar	325K	350K	375K	405K*	70%	80%	90%*	100%
10084	8.38	8.26	7.91	8.48	8.44	8.40	8.35	8.09	8.18	8.35	8.37
14259	8.15	8.03	7.80	8.24	8.19	8.14	8.08	7.88	8.01	8.08	8.24
15071	8.26	8.14	7.83	8.32	8.28	8.25	8.18	7.96	8.04	8.18	8.24
15201	8.21			8.24	8.22	8.15	8.21	8.00	8.07	8.21	8.26
15411	8.21			8.23	8.17	8.13	8.08	7.92	7.99	8.08	8.11
66031	8.11	8.02	7.82	8.16	8.11	8.07	8.02	7.89	7.94	8.02	8.04
67701	8.10	8.02	7.84	8.00	7.98	7.96	7.93	7.87	7.89	7.93	7.95
70181	8.40	8.29	8.02	8.48	8.42	8.38	8.34	8.13	8.21	8.34	8.36
72501	8.18			8.19	8.17	8.14	8.11	7.96	8.01	8.11	8.13
79221	8.35	8.23	7.92	8.53	8.53	8.48	8.57	8.10	8.25	8.57	8.47
Spectral Contrast (%) Max Uncertainty ± 0.36%											
10084	2.4	3.1	7.5	2.8	2.9	2.9	3.1	6.2	4.8	3.1	2.2
14259	2.9	4.3	26.5	3.8	4.1	4.4	4.9	10.0	6.0	4.9	2.9
15071	2.9	3.8	17.8	4.0	4.2	4.3	4.7	10.1	7.2	4.7	4.0
15201	3.3			5.3	5.4	5.9	4.9	7.7	7.2	4.9	4.3
15411	3.5			5.6	6.2	6.7	7.2	12.8	10.1	7.2	6.6
66031	3.3	5.1	33.0	5.6	6.1	6.5	7.3	14.0	10.8	7.3	6.6
67701	4.3	5.0	23.5	10.3	10.7	11.2	11.9	13.7	15.7	11.9	10.9
70181	2.1	2.4	5.1	3.1	3.3	3.6	3.7	6.6	5.3	3.7	3.3
72501	3.5			6.7	6.8	7.0	7.4	4.4	10.5	7.4	6.6
79221	2.6	3.5	8.7	2.6	2.5	2.6	2.4	6.5	4.3	2.4	2.2
Brightness Temps (K) Max Uncertainty ± 1.5 K											
10084	406.2	362.6	304.2	407.4	409.5	411.2	413.7	319.4	366.9	413.7	424.7
14259	409.0	367.6	306.8	388.1	389.9	393.0	396.9	331.3	378.1	396.9	443.8
15071	412.0	373.0	312.3	413.8	417.5	419.5	425.7	332.1	379.4	425.7	441.6
15201	397.4			367.4	367.7	368.8	404.8	307.5	357.6	404.8	421.3
15411	408.0			385.7	386.6	389.9	394.1	316.1	352.5	394.1	407.4
66031	409.4	370.5	308.3	390.4	392.9	395.5	399.6	308.9	354.4	399.6	409.2
67701	413.0	377.6	313.1	386.8	390.2	394.0	398.2	309.4	355.7	398.2	410.8
70181	404.5	361.1	303.1	410.4	413.2	414.4	416.0	317.7	366.8	416.0	428.2
72501	400.3			392.7	394.4	395.9	398.1	302.8	351.3	398.1	413.1
79221	406.5	364.9	300.0	421.7	422.9	424.7	426.8	328.3	377.2	426.8	444.1

* 405 K and 90%Lamp experimental conditions are the same measurement conditions.

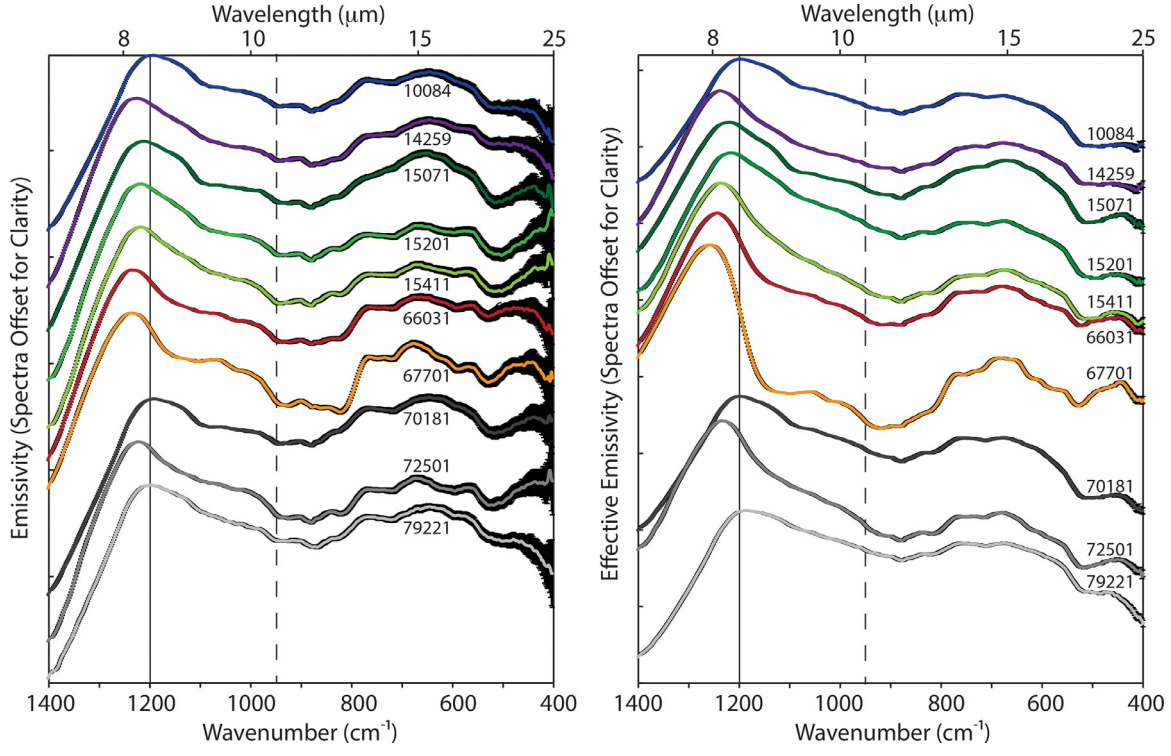

Fig. 7. (Left) Ambient spectral measurements of the suite of bulk lunar soil samples. Under ambient conditions samples were heated from below to 405 K, the interior chamber temperature was 297 K, and the chamber pressure was 1000 mbar. (Right) Simulated lunar environment (90% lamp in Table 5) spectral measurements of the same bulk lunar soil samples. Under simulated lunar environment conditions samples were heated from below to 405 K, the power of the solar-like halogen lamp was 160 W, the interior chamber temperature was 85 K, and the chamber pressure was $<10^{-4}$ mbar. Vertical solid line highlights the shift in CF position owing to composition and change in environmental conditions while the vertical dashed line at 10.5 μm marks the wavelength at which the CF to RB spectral contrast is calculated. In both plots, the uncertainties (1σ) in the thermal stability of the sample are expressed by the error bars.

Table 7
ALEC experimental conditions for San Carlos olivine spectral measurements.

	Sample cup Temp (K)	Lamp power (W)	Irradiance on sample (mW/cm^2)	Chamber pressure (mbar)	Chamber temp (K)
Ambient (Earth-like)	405 ± 0.2			980 ± 20	297 ± 2
325 K	325 ± 0.2	200 ± 0.1	146 ± 2	$<10^{-4}$	85 ± 0.5
350 K	350 ± 0.2	200 ± 0.1	146 ± 2	$<10^{-4}$	85 ± 0.5
375 K	375 ± 0.2	200 ± 0.1	146 ± 2	$<10^{-4}$	85 ± 0.5
405 K*	405 ± 0.2	200 ± 0.1	146 ± 2	$<10^{-4}$	85 ± 0.5
90% Lamp	405 ± 0.2	160 ± 0.1	129 ± 2	$<10^{-4}$	85 ± 0.5
100% Lamp*	405 ± 0.2	200 ± 0.1	146 ± 2	$<10^{-4}$	85 ± 0.5

*405 K and 100%Lamp experimental conditions are the same measurement conditions.
** Uncertainties in sample cup temperature, lamp power, chamber pressure, and chamber temperature are maximum uncertainties.

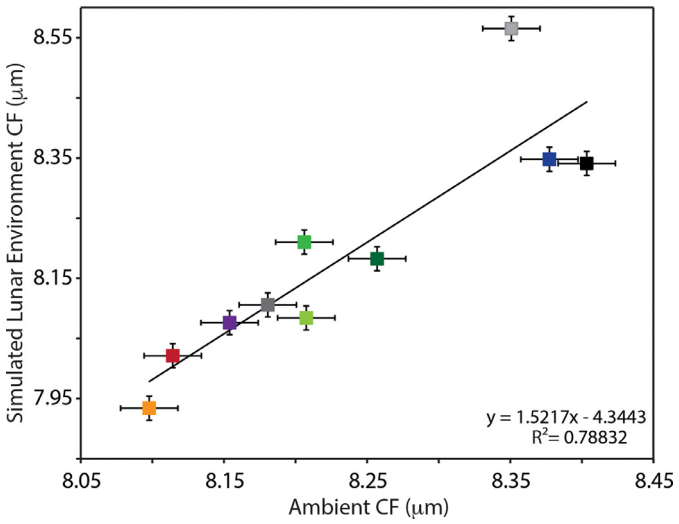

Fig. 8. Christiansen feature (CF) positions from spectral measurements of the bulk lunar soils measured under ambient conditions versus CF positions from spectral measurements of the same soils measured under simulated lunar environment (SLE) conditions (90% lamp in Table 5). Data symbols are color coordinated with spectra in Fig. 4. Error bars illustrate the maximum uncertainty in the CF position (0.02 μm) for both ambient and SLE measurements. (For interpretation of the references to color in this figure legend, the reader is referred to the web version of this article.)

325 K, 350 K, 375 K, 70% Lamp, 80% Lamp, and 100% Lamp) are provided in Figs. 1–8 in the Supplementary Materials. Our spectral measurements corroborate earlier studies of particulate rock, mineral separates, and lunar soils made under vacuum and lunar-like conditions (Logan and Hunt, 1970; Logan et al., 1973; Salisbury and Walter, 1989; Henderson et al., 1996; Thomas et al., 2012; Donaldson Hanna et al., 2012a, 2012b). Under Mars-like (5 mbar), vacuum, and simulated lunar conditions, the CF position shifts to shorter wavelengths (higher wavenumbers) and the spectral contrast between the CF and RB increases (see Table 6) when compared to spectra measured under Earth-like conditions. As seen in Fig. 6, spectral measurements of San Carlos olivine (particle size < 25 μm) made under simulated lunar conditions (90% Lamp conditions in Table 7) also show a shift in the CF position to shorter wavelengths and an increase in spectral contrast between the CF and RB. The observed shift in CF position for a pure mineral like San Carlos olivine (0.19 μm) is greater than the shifts observed in the lunar soils (0.1 ± 0.04 μm) and the observed increase in spectral contrast for olivine (13.3%) is greater than the increases in spectral contrast of the soils (4 ± 2%).

Previous laboratory studies have shown that the CF position measured under ambient conditions is linearly related to the CF position measured under vacuum and lunar-like conditions (Salisbury and Walter, 1989; Donaldson Hanna et al., 2012b). These laboratory studies focused on particulate (< 63 μm) rock and mineral samples. Fig. 8 demonstrates that the CF positions measured under ambient conditions relate linearly to CF positions measured under simulated lunar conditions, although the measurement of Apollo soil 79221 does affect the goodness of fit (it decreases the R^2 value of the linear regression). The slope of the linear regression through the lunar soil spectral measurements (1.52, Fig. 8) is different from the slopes through the particulate rock 0.90, (Donaldson Hanna et al., 2012b) and mineral 0.95, (Donaldson Hanna et al., 2012b) spectral measurements, but these differences likely result from differences in the experimental conditions under which they were measured. Particulate rock samples were measured under vacuum conditions (the atmospheric pressure inside the chamber was $<10^{-3}$ mbar, the samples were heated from below, and the chamber was not cooled) (Salisbury and Walter, 1989), while the particulate mineral samples were measured under lunar-like conditions (the atmospheric pressure inside the chamber was $<10^{-4}$ mbar, the samples were heated from below, and the chamber was cooled to temperatures < 125 K). Thus, the slope in the linear regression from our spectral measurements is not expected to be the same as the slope determined in previous studies.

5.1. Spectral effects due to varying pressure and temperature conditions

Previous laboratory studies focused on making laboratory emissivity measurements under a single near-surface environment (or a single thermal gradient) (e.g. Logan et al., 1973; Henderson et al., 1996; Henderson and Jakosky, 1997; Salisbury and Walter, 1989; Thomas et al., 2012; Donaldson Hanna et al., 2012a, 2012b). However in this work we focus on the spectral effects due to varying near-surface environments. Three Apollo soils (15071, 66031 and 67701) were chosen for detailed analysis as they represent units of different composition, mare (15071) versus highlands (66031 and 67701), and different soil maturities. Fig. 9 shows the spectral measurements of bulk lunar soils 15071, 66031 and 67701 measured under the temperature and pressure conditions outlined in Section 4 and in Table 5. In addition, Table 6 includes the CF position, the calculated spectral contrast between the CF and the RB, and the estimated brightness temperature for each of the lunar soils for each of the experimental conditions under which they were measured.

The top left plot in Fig. 9 shows results for mare-rich soil sample 15071 (I_s/FeO = 52) as the atmospheric pressure inside the chamber is systematically varied. The CF is observed to shift to shorter wavelengths (higher wavenumbers), the spectral contrast of the CF relative to the RB is enhanced, and the estimated brightness temperature of the sample decreases as the atmospheric pressure decreases from ambient (~1000 mbar) to vacuum ($<10^{-3}$ mbar) pressures. It is important to note that the CF is observed to shift to slightly shorter wavelengths (0.1 ± 0.02 μm) and the spectral contrast increases slightly (1 ± 0.3%) when the pressure decreases from ~1000 mbar (Earth-like atmospheric pressures) to ~5 mbar (Mars-like atmospheric pressures), suggesting that

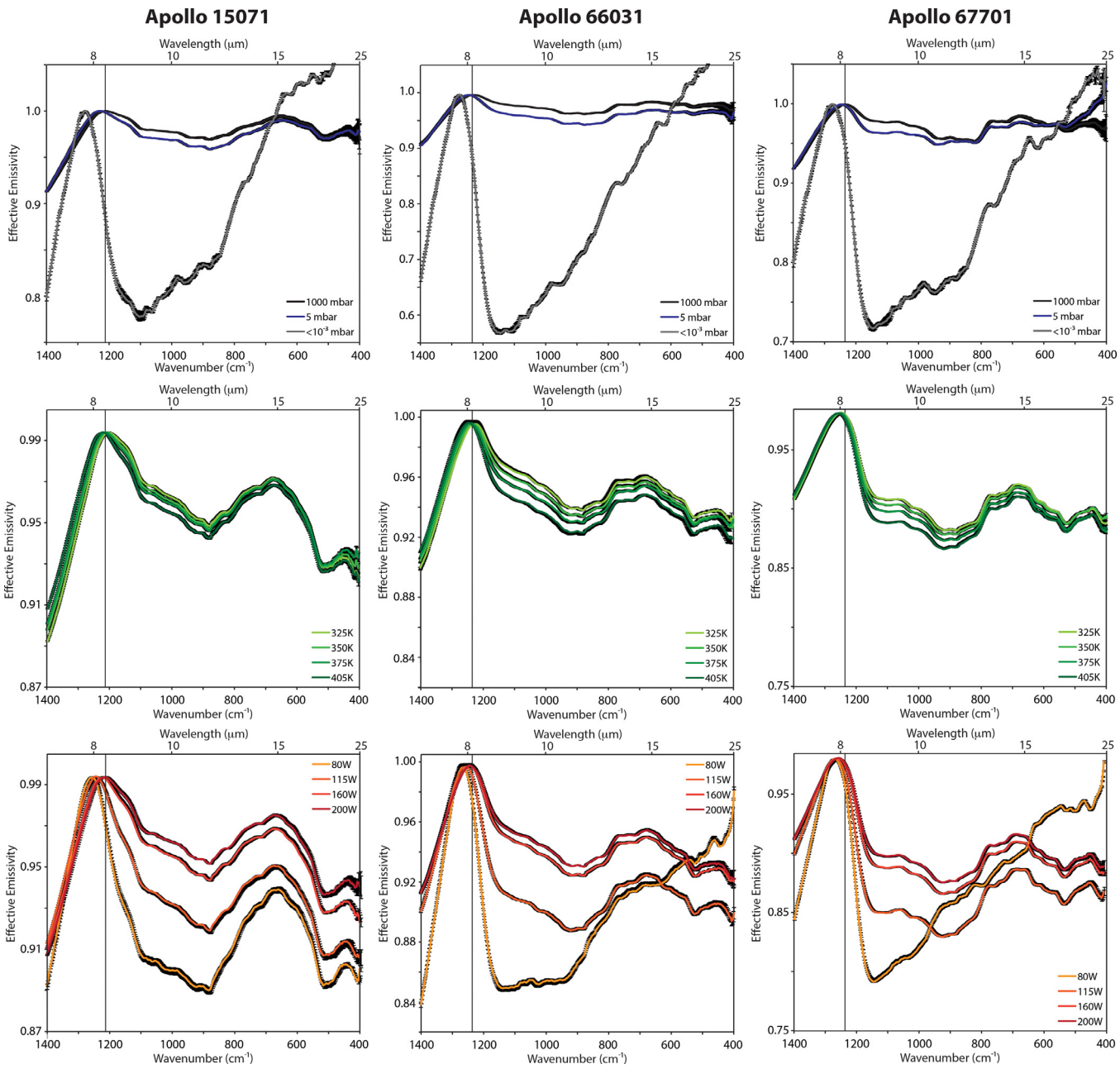

Fig. 9. Lunar soils 15071 (left), 66031 (middle), and 67701 (right) measured under varying conditions: internal chamber pressure, sample cup heater temperature, and solar lamp power. (Top) Internal chamber pressure was varied between 1000 mbar and $<10^{-3}$ mbar (vacuum pressures), the sample was heated to a constant temperature of 405 K, no heating from the solar lamp was applied, and the chamber was not cooled. (Middle) Sample cup heater temperature was varied between 325 K and 405 K, the power of the solar lamp was held constant at 160 W, the pressure was kept at vacuum pressures ($<10^{-4}$ mbar), and the chamber was cooled to 85 K. (Bottom) Power of the solar lamp was varied between 80 W and 200 W, the sample was heated to a constant temperature of 405 K, the pressure was kept at vacuum pressures ($<10^{-4}$ mbar), and the chamber was cooled to 85 K. In all plots, the uncertainties (1σ) in the thermal stability of the sample are expressed by the error bars.

spectral measurements of particulate materials on Mars-like surfaces may be affected by the atmospheric pressure.

The middle left plot shows results for Apollo soil sample 15071 as the sample cup temperature is systematically varied between 325 K and 405 K. The CF is observed to shift to slightly shorter wavelengths (0.14 μm), the spectral contrast of the CF relative to the RB slightly increases (0.7%), and the estimated brightness temperature of the sample slightly increases (12 K) as the sample cup temperature increases. All of the observed spectral differences due to sample cup temperature are subtle and much less pronounced than the spectral effects due to pressure. This confirms that the thermal gradient we are measuring is confined to the upper hundreds of microns and the sample cup heater, which is at a depth of 2 mm, has only a secondary effect on the thermal gradient that affects these spectral measurements.

As the power of the solar-like halogen lamp is increased from 80 to 200 W (increasing the irradiance on the sample from 52 to 146 mW/cm^2), the CF shifts to longer wavelengths (0.2 ± 0.05 μm), the spectral contrast of the CF relative to the RB decreases (5 ± 2%), and the brightness temperature of the sample increases (100 ± 10 K) as seen in the bottom left plot in Fig. 9 and in Table 5. This suggests that as the irradiance on the sample increases the CF position and spectral contrast in the spectral measurements trend closer to the CF position and spectral contrast in the ambient

measurements. The observed spectral differences due to the solar-like radiation incident on the surface of the sample are similar in scale to the differences due to pressure, suggesting these are the two dominant factors in establishing the thermal gradient formed in the near-surface regolith.

Fig. 9 also includes spectral measurements for highland soil samples 66031 (I_s/FeO = 102) and 67701 (I_s/FeO = 39). The observed spectral differences due to systematically varying the atmospheric pressure, sample cup temperature and solar-like incident radiation are similar to those observed in spectral measurements of Apollo 15071. However, the estimated brightness temperatures for the highlands soil samples are lower (on the order of 10–20 K) than mare-rich soils like 15071. The observed differences in the brightness temperature are likely due to the inherent difference in albedo of the soils owing to their mineralogy (Lucey et al., 2016).

Spectral measurements of San Carlos olivine (particle size < 25 μm) were also made under varying environmental conditions (Table 7) for comparison with the lunar soils spectral measurements. Measurements under vacuum conditions were not possible as the signal from the sample was too low to measure above the ambient temperature of the FTIR. Thus, spectral changes due to changes in atmospheric pressure inside the chamber cannot be evaluated here. In addition, only the 90%Lamp and 100%Lamp settings heated the sample enough for a signal to be measured over the ambient temperature of the FTIR. Fig. 10 illustrates the spectral effects due to changes in the sample cup temperature and the power of the solar lamp. As the sample cup temperature is systematically varied between 325 K and 405 K, the CF is observed to shift to slightly shorter wavelengths (0.04 μm), the spectral contrast of the CF relative to the RB slightly increases (0.02%), and the estimated brightness temperature of the sample increases (18 K). The observed differences in the spectra are smaller than those observed for the lunar soils as the sample cup temperature was varied. As the power of the solar lamp was varied between 160 and 200 W, the CF is observed to shift to slightly longer wavelengths (0.02 μm), the spectral contrast of the CF relative to the RB slightly decreases (0.9%), and the estimated brightness temperature of the sample slightly increases (7 K). Again, the observed differences in the olivine spectra (Table 8) are smaller than those observed for the lunar soils (Table 6).

5.2. Spectral effects due to space weathering

The two highlands lunar soil samples included in this study, 66031 and 67701, have similar normalized modal phase contents (Table 3) (Taylor et al., 2012) and relatively similar bulk compositions (Table 4; i.e. low FeO, and high CaO and Al_2O_3) (Korotev 1982; Rose et al., 1975), but different maturities (Table 2) (Morris, 1978). In fact, when the modal contents of the soils are normalized after the glass component has been removed the plagioclase contents in 66031 and 67701 are 81.0 and 86.4%, respectively (Taylor et al., 2012). Thus, spectral measurements of these two soils can provide an initial understanding of the effects of space weathering on TIR emissivity spectra. Spectral measurements of both soils under ambient conditions have similar CF positions (8.11 μm versus 8.10 μm), but the spectrum of immature soil 67701 has slightly greater spectral contrast (4.3% versus 3.3%) than the spectrum of mature soil 66031 (see Fig. 11 and Table 6). Under simulated lunar conditions, however, the CF position of immature soil 67701 has shifted to shorter wavelengths than the CF of mature soil 66031 (7.93 μm versus 8.02 μm), and the spectral contrast between the CF and RB is much greater (11.9% versus 7.3%) in the immature, higher albedo soil sample. These initial results suggest that space weathering has observable effects on TIR emissivity spectra measured under simulated lunar conditions. These effects, in particular the observation that maturity affects the wavelength position

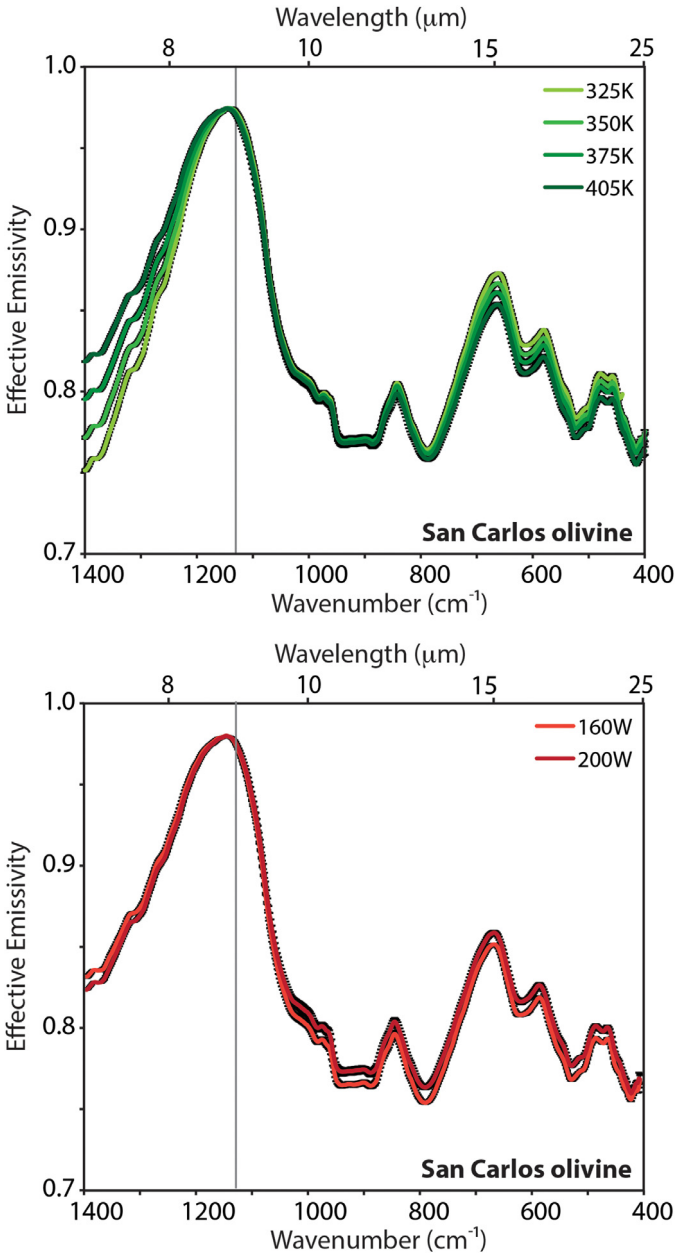

Fig. 10. Simulated lunar environment measurements of San Carlos olivine (<25 μm). (Top) Sample cup heater temperature was varied between 325 K and 405 K, power of the solar lamp was held constant at 200 W, the pressure was kept at vacuum pressures (<10^{-4} mbar), and the chamber was cooled to 85 K. (Bottom) Power of the solar lamp was varied between 160 W and 200 W, the sample was heated to a constant temperature of 405 K, the pressure was kept at vacuum pressures (<10^{-4} mbar), and the chamber was cooled to 85 K. In all plots, the uncertainties (1σ) in the thermal stability of the sample are expressed by the error bars.

of the CF, are similar to those observed in the Diviner TIR observations of immature locations like crater ejecta rays and the more mature surface locations the ejecta deposits are emplaced on Lucey et al., (2016).

5.3. Comparison of laboratory spectra with Diviner TIR observations

To constrain the laboratory conditions in ALEC that best simulate the near-surface environment of the Moon, spectral measurements of lunar soils under varying conditions are compared with Diviner thermal infrared observations of the Apollo landing sites, in particular the sampling sites where specific lunar samples used

Table 8
San Carlos olivine CF positions (μm), spectral contrast (%) and brightness temperatures (K).

CF Positions (μm) Max Uncertainty ± 0.02 μm	1000 mbar	325K	350K	375K	405K*	90%	100%*
Olivine	8.88	8.75	8.74	8.72	8.71	8.69	8.71
Spectral Contrast (%) Max Uncertainty ± 0.36%							
Olivine	7.5	19.7	19.8	19.8	19.9	20.8	19.9
Brightness Temps (K)							
Olivine	343.1 ± 0.1	322.5 ± 0.1	328.0 ± 0.8	333.7 ± 1.5	340.6 ± 1.5	333.1 ± 1.3	340.6 ±1.5

* 405 K and 100%Lamp experimental conditions are the same measurement conditions.

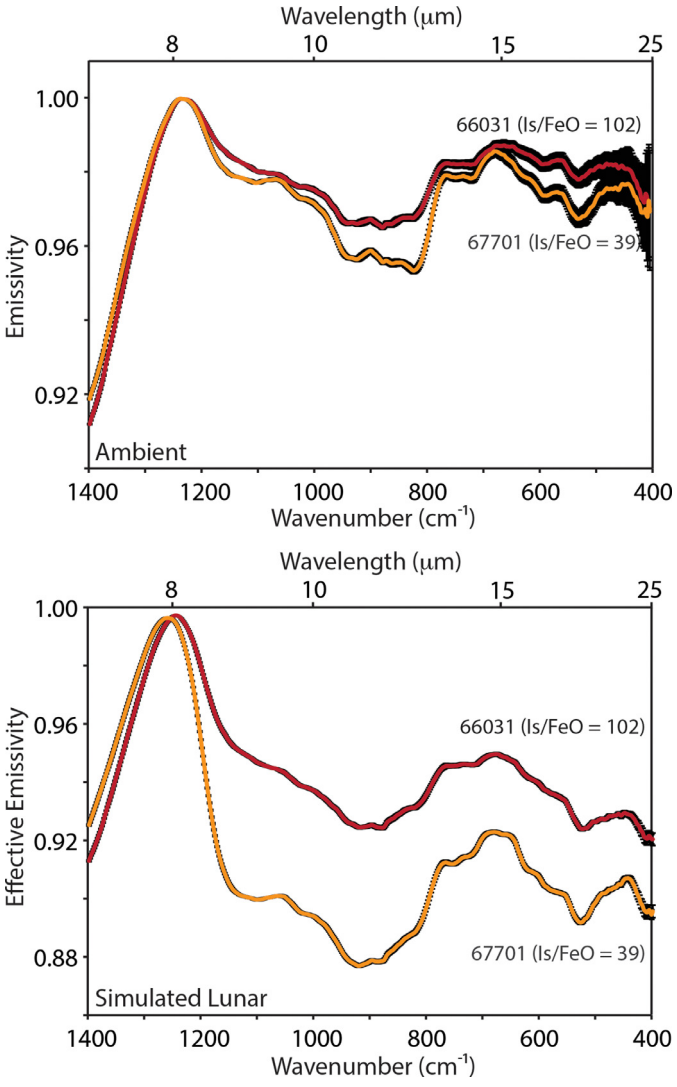

Fig. 11. (Top) Ambient spectral measurements of mature lunar soil 66031 and immature lunar soil 67701. Under ambient conditions samples are heated from below to 405 K, the interior chamber temperature was 297 K, and the chamber pressure was 1000 mbar. **(Bottom)** Simulated lunar environment spectral measurements of the same bulk lunar soil samples (90% Lamp in Table 5)**.** Under simulated lunar environment conditions samples are heated from below to 405 K, the power of the solar-like halogen lamp was 160 W, the interior chamber temperature was 85 K, and the chamber pressure $<10^{-4}$ mbar. In both plots, the uncertainties (1σ) in the thermal stability of the sample are expressed by the error bars.

in this study were collected. In Figs 12 and 13, albedo maps of the Apollo 15 and 16 landing sites, including the traverse maps and location of sampling stations, are overlain with Diviner CF maps of each region (Greenhagen et al., 2012). A cyan-colored arrow in Fig. 12 indicates Apollo 15 sampling station 1 near Elbow crater, which is near the turn in Hadley Rille and at the boundary of the mare surface with the Apennine Front. Bulk soil sample 15071 was collected 20 m from the rim of Elbow crater. Yellow arrows in Fig. 13 indicate Apollo 16 sampling stations 6 and 11 where bulk samples 66031 and 67701 were collected, respectively. Soil sample 66031 was collected on the Cayley Plain near Stone Mountain and may include a small component of South Ray crater ejecta. Apollo sample 67701 was collected on the rim of North Ray crater approximately half way between House Rock and Boulder 'B'. Average Diviner emissivity spectra are extracted from 400 m boxes enclosing each of the sampling sites and are compared to laboratory spectra of samples 15071, 66031 and 67701.

In Fig. 12, the average Diviner emissivity spectrum for this mare-rich region is plotted along with the re-sampled laboratory spectra of bulk lunar soil 15071 measured when the power of the solar lamp was varied between 80 and 200 W (irradiance on sample varied between 52 and 146 mW/cm^2). The maximum uncertainty in the re-sampled laboratory emissivity spectra are plotted in Fig. 12, but are smaller than the size of the data symbols. The spectrum of 15071 with the solar lamp power set to 160 W and a calculated brightness temperature of 425.7 K is within the standard deviation of the average Diviner emissivity spectrum of Apollo 15 sampling station 1. As seen in the re-sampled laboratory spectra of Apollo 15071, as the power of the solar lamp and the brightness temperature of the sample increases the emissivity at 7.81 μm decreases and the emissivity at 8.6 μm increases. This suggests that the solar lamp power could be finely tuned between 115 W and 160 W to obtain spectra that have a brightness temperature closer to those of the lunar surface and are a better spectral match to the Diviner observations.

In Fig. 13, re-sampled laboratory emissivity spectra of highland bulk lunar soils 66031 and 67701 are compared with average Diviner emissivity spectra of Apollo sampling stations 6 and 11. Again, the maximum uncertainties in the re-sampled laboratory spectra are plotted in Fig. 12, but are smaller than the size of the data symbols. The spectrum of very mature soil 66031 with the solar lamp power set at 200 W and a calculated brightness temperature of 409.2 K is within two standard deviations of the average Diviner emissivity spectrum of Apollo 16 sampling station 6, whereas the spectrum of immature soil 67701 with solar lamp power set at 200 W and a calculated brightness temperature of 410.8 K is not within two standard deviations of the average Diviner emissivity spectrum of Apollo 16 sampling station 11. These initial results suggest that even when using the highest power on ALEC's solar lamp it is difficult to simulate near-surface conditions for immature highlands samples when compared to Diviner observations, likely due to their higher albedos. Our results for the first measurements of highlands and mare bulk lunar soils measured in ALEC demonstrate that re-sampled laboratory spectra of mature bulk lunar soils are within two standard deviations of the average Diviner emissivity spectra of the specific Apollo sampling sites.

6. Discussion and future work

Our initial results corroborate previous lab measurements of particulate samples (<63 μm) showing the sensitivity of thermal

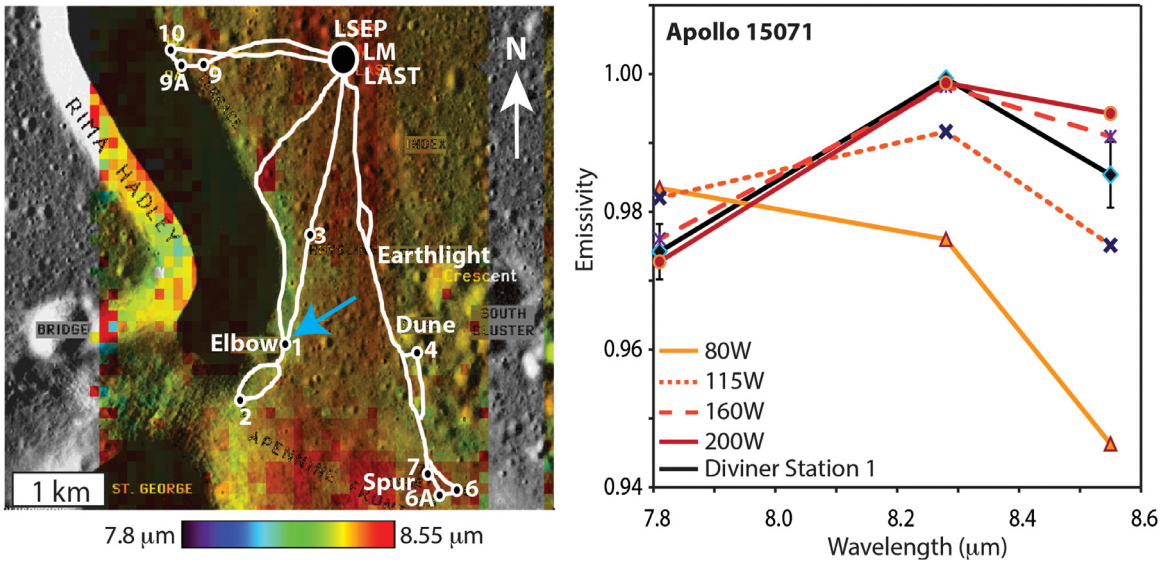

Fig. 12. (Left) Apollo 15 landing site and traverse map (Defense Mapping Agency Topographic Center (DMATC) map 41B4S4) overlain with Diviner CF observations for the region. The cyan arrow indicates sampling station 1 on the ejecta blanket of Elbow crater where Apollo 15071 was collected. (Right) An average Diviner emissivity spectrum for a 400 m box enclosing Apollo 15 sampling station 1 plotted along with the laboratory spectra of Apollo 15071 measured under varying solar lamp power. Full resolution lab spectra were re-sampled to Diviner's three '8 μm' bands. The *y*-error bars on the Diviner emissivity spectrum represent the standard deviation (1σ) of the emissivity for each Diviner band. The *y*-error bars on the re-sampled laboratory spectra represent the standard deviation (1σ) of the sample measurements due to thermal stability. These *y*-error bars are smaller than the data symbols. (For interpretation of the references to color in this figure legend, the reader is referred to the web version of this article.)

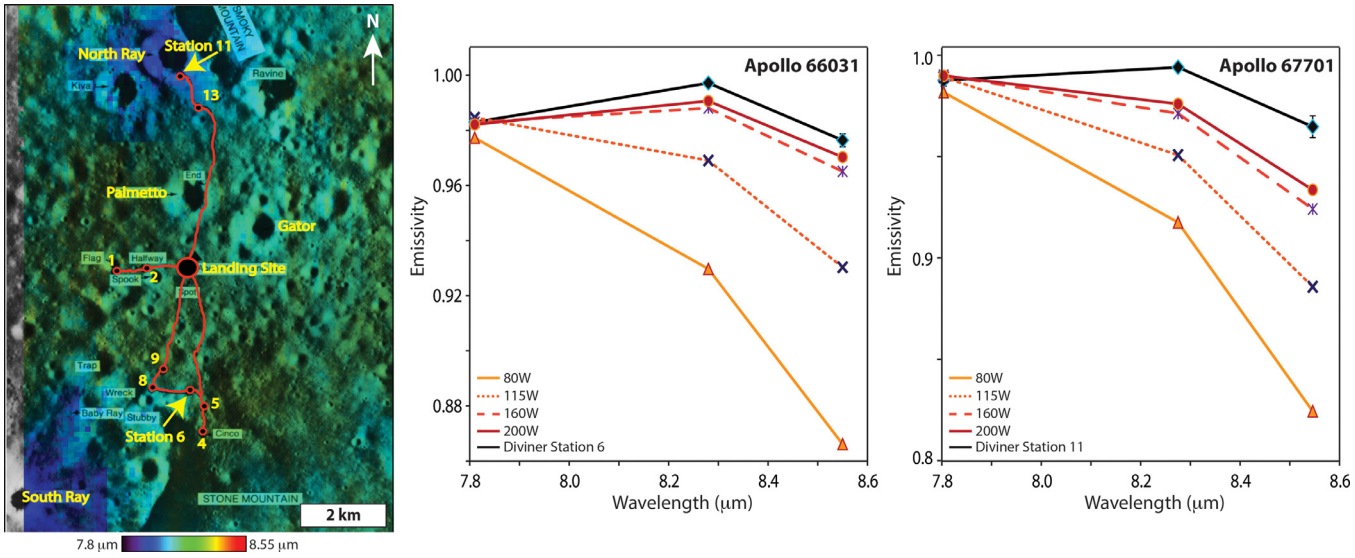

Fig. 13. (Left) Apollo 16 landing site and traverse map (Defense Mapping Agency Topographic Center (DMATC) map 78D2S2) overlain with Diviner CF observations for the region. The yellow arrows indicate sampling stations 6 and 11 where Apollo bulk lunar soils 66031 and 67701 were collected, respectively. (Middle) An average Diviner emissivity spectrum for a 400 m box enclosing Apollo 16 sampling station 6 plotted along with the laboratory spectra of Apollo 66031 measured under varying solar lamp power. Full resolution lab spectra were re-sampled to Diviner's three '8 μm' bands. The *y*-error bars on the Diviner emissivity spectrum represent the standard deviation (1σ) of the emissivity for each Diviner band. The *y*-error bars on the re-sampled laboratory spectra represent the standard deviation (1σ) of the sample measurements due to thermal stability. (Right) An average Diviner emissivity spectrum for a 400 m box enclosing Apollo 16 sampling station 11 plotted along with the laboratory spectra of Apollo 67701 measured under varying solar lamp power. Full resolution lab spectra were re-sampled to Diviner's three '8 μm' bands. The *y*-error bars on the Diviner emissivity spectrum represent the standard deviation of the emissivity for each Diviner band. The *y*-error bars on the re-sampled laboratory spectra represent the standard deviation of the sample measurements due to thermal stability. In the middle and right figures the *y*-error bars on the re-sampled lab spectra are smaller than the data symbols. (For interpretation of the references to color in this figure legend, the reader is referred to the web version of this article.)

infrared emissivity spectra to the conditions under which they are measured and for the first time characterizing how varying the solar-like irradiance on the sample changes the TIR emissivity spectra. The two parameters that introduce the greatest changes to the spectral measurements are the atmospheric pressure inside the chamber and the power of the solar lamp (incident solar-like radiation on the sample). As atmospheric pressure decreases, the abundance of interstitial gases between grains is reduced and heat is no longer efficiently transferred through conduction, but rather is transferred through radiation. Due to the fine particulate nature of the sample and low pressure, heat is not transferred efficiently from the bottom of the heated sample cup to the top of the sample exposed to the environment in the chamber, thus setting up a thermal gradient in the sample and causing spectral differences.

As seen in Fig. 9, even at pressures similar to atmospheric conditions on Mars (~5 mbar) differences are observed in the position of the CF and the spectral contrast between the CF and the RB when compared to spectra measured under Earth-like conditions. Thus, changing only the atmospheric pressure inside the chamber can induce small, but detectable changes in the laboratory spectra of particulate samples.

As the power of the solar lamp (or incident solar-like radiation) is systematically increased, it is observed that (1) the calculated brightness temperature of the sample systematically increases, (2) the CF shifts slightly to lower wavenumbers (longer wavelengths), and (3) the spectral contrast between the CF and RB decreases. These observations suggest that as fine particulate samples are heated to higher brightness temperatures, particulates more efficiently transfer heat to surrounding particulates due to an increase in the radiative transfer of heat at higher temperatures (e.g. Vasavada et al., 1999). While previous laboratory studies have focused on making laboratory emissivity measurements under a single near-surface environment (or a single thermal gradient) (e.g. Logan et al., 1973; Henderson et al., 1996; Henderson and Jakosky; 1997), our results show that to directly compare laboratory measurements to remote sensing data from airless bodies like the Moon, Mercury, and asteroids the correct near-surface environment (thermal gradient) needs to be simulated in the laboratory.

To better interpret surface compositions from thermal infrared observations like those from Diviner, laboratory measurements made under simulated lunar conditions of Apollo soil samples, lunar meteorites and pure mineral analogues requires continued refinement. While this work illustrates that ALEC is capable of simulating near-surface conditions similar to those on the Moon, future laboratory work will focus on measuring a wider range of lunar soil compositions and maturities and fine tuning the environmental conditions to find the 'best' laboratory conditions for simulating the near-surface environment of the Moon. In addition, thermal infrared spectral effects due to particle size, porosity/sample packing, and space weathering need to be further investigated under simulated lunar conditions.

The first consideration is the effect of particle size on thermal infrared emissivity spectra and in particular which particle size fraction dominates the spectral signature. Detailed analyses of lunar soil samples have shown that reflectance measurements across the visible- to near-infrared wavelengths are dominated by the finest particle size fraction (< 45 μm) (e.g. Pieters et al., 1993, Fischer, 1995). However, it has yet to be demonstrated what particle size fraction dominates the spectra of the bulk lunar soil samples and the Diviner thermal infrared observations.

Another consideration is the effect of porosity on TIR emissivity spectra as the 'fluffiness' of the lunar near-surface is often termed a 'fairy-castle' structure (Hapke and Van Horn, 1963). Often, porosity is simulated in the laboratory by varying the way a sample is packed into a sample cup. Laboratory studies of ambient thermal infrared reflectance measurements by Salisbury and Wald (1992) demonstrated that the porosity or packing of the sample in the sample cup affects the wavelength position of the CF and the spectral contrast in the RB region. As samples become more porous or fluffy, the CF shifts to slightly longer wavelengths and the spectral contrast in the RB region decreases. Recent studies of bulk lunar soil Apollo 15071 prepared with four different packing styles and measured under simulated lunar conditions in the Simulated Lunar Environment Chamber at the University of Oxford by Donaldson Hanna et al. (2015b) corroborate results by Salisbury and Wald (1992). However, a more detailed study on a suite of well-characterized samples is needed to constrain the porosity/packing style that best simulates the surface texture on the Moon and to understand how laboratory measurements compare to remote sensing observations of undisturbed lunar soils in their native setting.

The effect of space weathering on TIR emissivity is another vital consideration for future laboratory studies as the entire lunar surface has experienced some degree of space weathering. A study of thermal infrared reflectance measurements of plagioclase feldspars demonstrated that the vitrification process does not affect the position of the CF (Nash and Salisbury, 1991; Nash et al., 1993). This led many to believe that effects on TIR emissivity spectra due to space weathering would not be observed. However, Lucey et al. (2016) have demonstrated that space weathering does strongly influence the position of the CF as observed in Diviner observations. To constrain fully the effects of space weathering on TIR emissivity spectra a detailed laboratory study under simulated lunar conditions is needed. Our results for an immature highlands soil sample and a very mature highlands soil sample indicate that as a soil matures the position of the CF shifts to slightly longer wavelengths and the spectral contrast of the RB decrease, but these are just two bulk lunar soils. Additional lunar highlands and mare soil pairs (similar compositions, but different maturities) need to be measured under simulated lunar conditions to fully characterize the spectral effects associated with space weathering.

In addition to the considerations outlined above, laboratory measurements of lunar soils and other analogue materials made in ALEC need to be compared with measurements made under simulated lunar conditions in other laboratories. Laboratories with the capability of making thermal infrared emissivity measurements under simulated airless body conditions include the Simulated Lunar Environment Chamber (SLEC) in the Planetary Spectroscopy Facility at the University of Oxford (Thomas et al., 2012), the Simulated Airless Body Emission Laboratory (SABEL) at Johns Hopkins University Applied Physics Laboratory (APL), the Planetary and Asteroid Regolith Spectroscopy Environmental chamber (PARSEC) in the Vibrational Spectroscopy Laboratory at Stony Brook University (Shirley and Glotch, 2015), and the Planetary Emissivity Laboratory (PEL) at DLR (the German Aerospace Center) (Maturilli et al., 2006). Cross-laboratory measurements of the same suite of well-characterized lunar soils are vital to (1) understand the observed spectral differences resulting from different laboratory set-ups, (2) constrain the 'best' measurement practices across laboratories enabling direct comparisons of spectral measurements, and (3) build spectral libraries of lunar soils, lunar meteorites, and analogue mineral separates and mixtures for the community to use in the analyses of remote sensing data of the Moon. Initial comparisons of Apollo soil 15071 measured under simulated lunar conditions in ALEC and SLEC show that all of the major spectral features (CF, RB and TF) are observed at the same wavelengths, but differences on the order of 2% in the spectral contrast and slope are also observed (Donaldson Hanna et al., 2015a). The observed differences could arise from sample preparation as packing plays an important role in the spectral contrast of the RB (Salisbury and Wald, 1992), differences in the simulated near-surface environment in the two chambers, and/or from the calibration procedures of the two chambers (including the accounting for down welling radiance, if it is a measurable effect). The spectral differences observed between ALEC and SLEC measurements need to be further characterized to (1) understand where the differences arise and (2) minimize those differences as much as possible. The suite of well-characterized lunar soils will also be measured under simulated lunar conditions at APL's SABEL and Stony Brook's PARSEC in an effort to better characterize cross-laboratory measurement differences with those labs.

One of the ultimate goals of these laboratory studies is to measure the actual thermal gradient formed in the particulate samples under different environmental conditions to better constrain the thermal properties of the Moon's upper regolith. To accomplish

this goal new ALEC sample cups will need to be designed and built to accommodate temperatures sensors at the surface of the sample and at several depths within the upper hundreds of microns of the sample. Approximating the thermal gradient in the upper hundreds of microns in the lunar regolith by comparing lab measurements and Diviner observations will provide important constraints for modeling the thermophysical properties of the lunar surface (i.e. heat flow, the thickness of the "fluffy" low-density layer of the regolith, and the retention and mobility of volatiles in the regolith) as well as constraining the thermal gradients on other airless bodies.

7. Conclusions

Spectral measurements of a suite of well-characterized lunar soil samples made under ambient and simulated lunar conditions in the Asteroid and Lunar Environment Chamber (ALEC) corroborate previous laboratory spectral measurements of lunar soils, particulate rocks and minerals under vacuum and lunar-like conditions. These laboratory measurements highlight the sensitive nature of fine particulate materials to the environmental conditions in which they are measured and demonstrate that to compare laboratory measurements to remote sensing data from airless bodies like the Moon, Mercury, Mars' moons (Phobos and Deimos), and asteroids an appropriate near-surface environment (thermal gradient) needs to be simulated in the laboratory. As the atmospheric pressure inside the chamber is systematically varied between ambient (1000 mbar) and vacuum ($<10^{-3}$ mbar) pressures, the Christiansen Feature (CF) is observed to shift to shorter wavelengths (higher wavenumbers) and the spectral contrast of the CF relative to the reststrahlen bands (RB) is enhanced. As the power of the solar-like halogen lamp is increased from 80 to 200 W (irradiance 52–146 mW/cm^2), the CF shifts to longer wavelengths (lower wavenumbers) and the spectral contrast of the CF relative to the RB decreases. Changes in the pressure and halogen lamp power lead to competing spectral effects on the same scale. Spectral effects due to varying the sample cup temperature are subtle in comparison.

Spectral measurements of a fine particulate (<25 μm) sample of San Carlos olivine were measured under ambient and simulated lunar conditions to highlight the differences in behavior between lunar soils and pure mineral spectra. When comparing ambient and simulated lunar spectra, the observed shift in CF position for olivine (0.19 μm) is greater than the shifts observed in the lunar soils (0.1 ± 0.04 μm) and the observed increase in spectral contrast for olivine (13.3%) is greater than the increases in spectral contrast of the soils (4 ± 2%). However, under simulated lunar conditions as the sample cup temperature and incident solar-like radiation are varied the olivine spectra show little change in the CF position (0.04 μm and 0.02 μm, respectively) and spectral contrast between the CF and RB (0.02% and 0.9%, respectively). Due to the observed spectral differences between pure mineral spectra and bulk lunar soil spectra, caution should be used when using spectral measurements of pure minerals to interpret spectral features in thermal infrared observations like those from Diviner.

Finally, spectral measurements of bulk lunar soils under varying environmental conditions are compared with Diviner thermal infrared observations of the Apollo sampling stations to constrain laboratory conditions that 'best' simulate the near-surface of the Moon. Re-sampled laboratory emissivity spectra of mature lunar soils show that samples heated from above using solar lamp powers of 160 and 200 W (irradiance ~129 and 146 mW/cm^2) are within two standard deviations of the average Diviner emissivity spectra of the specific Apollo sampling sites. These results place important constraints for setting up the appropriate temperature and pressure conditions for future laboratory experiments that investigate the spectral effects of particle size, packing/porosity, space weathering, etc.

Acknowledgments

The authors thank Ian Thomas for the many helpful discussions during the installation, testing, and first light measurements of ALEC and Alessandro Maturilli and Jörn Helbert for the slag material used for the calibration of the spectral measurements. Daniel Moriarty and Takahiro Hiroi were invaluable in the installation and alignment of ALEC on many occasions. The authors thank Dr Katherine Joy and an anonymous reviewer for their thoughtful comments and thorough reviews, which greatly improved the manuscript. Donaldson Hanna was supported through NASA grant NNX08AM75G, the Solar System Exploration Research Virtual Institute (SSERVI) grant number NNA14AB01A, and Leverhulme Trust research grant RPG-2012-814 for this work. This is SSERVI publication number SSERVI-2016-0073.

Supplementary materials

Supplementary material associated with this article can be found, in the online version, at doi:10.1016/j.icarus.2016.05.034.

References

Allen, C.C., Greenhagen, B.T., Donaldson Hanna, K.L., et al., 2012. Analysis of lunar pyroclastic deposit FeO abundances by LRO Diviner. J. Geophy. Res. 117. doi:10.1029/2011JE003982.

Bandfield, J.L., Hayne, P.O., Williams, J.-P., et al., 2014. Lunar surface roughness derived from LRO Diviner radiometer observations. Icarus 357–372. doi:10.1016/j.icarus.2014.11.009.

Bandfield, J.L., Ghent, R.R., Vasavada, A.R., et al., 2011. Lunar surface rock abundance and regolith fines temperatures derived from LRO Diviner radiometer data. J. Geophy. Res. doi:10.1029/2011JE003866.

Basu, A., McKay, D.S., Griffiths, S.A., et al., 1981. Regolith maturation on the Earth and the Moon with an example from Apollo 15. In: Proc. Lunar Planet. Sci. Conf., 12, pp. 433–449.

Conel, J.E., 1969. Infrared emissivities of silicates: Experimental results and a cloudy atmospheric model of spectral emission from condensed particulate mediums. J. Geophy. Res. 74, 1614–1634.

Cooper, B.L., Salisbury, J.W., Killen, R.M., et al., 2002. Mid infrared spectra features and their powders. J. Geophy. Res. 107 (E4). doi:10.1029/2000JE001462.

Cuttitta, F., Rose, H.J., Annell, C.S., et al., 1973. Chemistry of twenty-one igneous rocks and soils returned by the Apollo 15 mission. In: Proc. 4th Lunar Sci. Conf., pp. 1081–1096.

Donaldson Hanna, K.L., Bowles, N.E., Pieters, C.M., et al., 2015. Thermal infrared emission studies of bulk Apollo soils: The importance of cross-laboratory analyses. In: Proc. Lunar Planet. Sci. Conf., 46, p. 1377.

Donaldson Hanna, K.L., Bowles, N.E., Pieters, C.M., et al., 2015. Simulating near surface lunar conditions in the lab: Applications to Diviner thermal infrared observations of the Moon. Eur. Lunar Symp. 3.

Donaldson Hanna, K.L., Cheek, L.C., Pieters, C.M., et al., 2014. Global assessment of pure crystalline plagioclase across the Moon and implications for the evolution of the primary crust. J. Geophy. Res. 119. doi:10.1002/2013JE004476.

Donaldson Hanna, K.L., Thomas, I.R., Bowles, N.E., et al., 2012. Laboratory emissivity measurements of the plagioclase solid solution series under varying environmental conditions. J. Geophys. Res. 117, E11004. doi:10.1029/2012JE004184.

Donaldson Hanna, K.L., Wyatt, M.B., Thomas, I.R., et al., 2012. Thermal infrared emissivity measurements under a simulated lunar environment: Application to the Diviner Lunar Radiometer Experiment. J. Geophy. Res. 117. doi:10.1029/2011JE003862.

Duncan, A.R., Sher, M.K., Abraham, Y.C., et al., 1975. Interpretation of the compositional variability of Apollo 15 soils. In: Proc. 6th Lunar Sci. Conf., pp. 2309–2320.

Feeley, K.C., Christensen, P.R., 1999. Quantitative compositional analysis using thermal emission spectroscopy: Application to igneous and metamorphic rocks. J. Geophy. Res. 104, 24195–24210.

Fischer, E.M., 1995. Ph.D. dissertation. Brown University, Providence, RI.

Foote, E.J., Paige, D.A., Shepard, M.K., et al., 2012. Laboratory and Diviner bidirectional reflectance measurements of Apollo soils. In: Proc. Lunar Planet. Sci. Conf., 43, p. 1659.

Fröhlich, C., 2006. Solar irradiance variability since 1978. Space Sci. Rev. 125, 53–65.

Ghent, R.R., Hayne, P.O., Bandfield, J.L., et al., 2014. Constraints on the recent rate of lunar ejecta breakdown and implications for crater ages. Geology 42, 1059–1062. doi:10.1130/G35926.1.

Glotch, T.D., Bandfield, J.L., Lucey, P.G., et al., 2015. Formation of lunar swirls by magnetic field standoff of the solar wind. Nature Commun. 6. doi:10.1038/ncomms7189.

Glotch, T.D., Hagerty, J.J., Lucey, P.G., et al., 2011. The Mairan domes: Silicic volcanic constructs on the Moon. Geophys. Res. Lett. 38. doi:10.1029/2011GL049548.
Glotch, T.D., Lucey, P.G., Bandfield, J.L., et al., 2010. Highly silicic compositions on the Moon. Science 329, 1510–1513. doi:10.1126/science.1192148.
Graf, J.C. (1993), Lunar soils grain size catalog, NASA Reference Publication 1265.
Greenhagen, B.T., Hayne, P.O., Paige, D.A., et al., 2015. Using lunar eclipses to investigate the regolith boundary layer. In: Proc. Lunar Planet. Sci. Conf., 46, p. 2949.
Greenhagen, B.T., Thomas, I.R., Bowles, N.E., et al., 2012. Compositional ground truth of Diviner lunar radiometer observations. In: Proc. Lunar Planet. Sci. Conf.,, 43, p. 2092.
Greenhagen, B.T., Lucey, P.G., Bandfield, J.L., et al., 2011. The Diviner lunar radiometer compositional data products: Description and examples. In: Proc. Lunar Planet. Sci. Conf., 42, p. 2679.
Greenhagen, B.T., Lucey, P.G., Wyatt, M.B., et al., 2010. Global silicate mineralogy of the Moon from the Diviner Lunar Radiometer. Science 329, 1507–1509. doi:10.1126/science.1192196.
Hamilton, V.E., 2000. Thermal infrared emission spectroscopy of the pyroxene mineral series. J. Geophy. Res. 105, 9701–9716.
Hamilton, V.E., Christensen, P.R., 2000. Determining modal mineralogy of mafic and ultramafic igneous rocks using thermal emission spectroscopy. J. Geophy. Res. 105, 9717–9734.
Hapke, B., Van Horn, H., 1963. Photometric studies of complex surfaces, with applications to the Moon. J. Geophys. Res. 48, 4545–4570.
Heiken, G.H., McKay, D.S., 1974. Petrography of Apollo 17 soils. In: Proc. 5th Lunar Sci. Conf., 1, pp. 843–860.
Henderson, B.G., Jakosky, B.M., 1997. Near-surface thermal gradients and mid-IR emission spectra: A new model including scattering and application to real data. J. Geophys. Res. 102, 6567–6580.
Henderson, B.G., Jakosky, B.M., 1994. Near-surface thermal gradients and their effects on mid-infrared emission spectra of planetary surfaces. J. Geophys. Res. 99 (E9), 19,063–19,073.
Henderson, B.G., Lucey, P.G., Jakosky, B.M., 1996. New laboratory measurements of mid-IR emission spectra of simulated planetary surfaces. J. Geophys. Res. 101, 14969–14975.
Hunt, G.R., Salisbury, J.W., 1964. Lunar surface features: Mid-infrared spectral observations. Science 146, 641–642.
Isaacson, P.J., Basu Sarbadhikari, A., Pieters, C.M., et al., 2011. The lunar rock and mineral characterization consortium: Deconstruction and integrated mineralogical, petrologic, and spectroscopic analyses of mare basalts. Meteor. Planet. Sci. 46, 228–251. doi:10.1111/j.1945-5100.2010.01148.x.
Johnson, J.R., Shepard, M.K., Grundy, W.M., et al., 2013. Spectrogoniometry and modelling of martian and lunar analog samples and Apollo soils. Icarus 223, 383–406. doi:10.1016/j.icarus.2012.12.004.
King Jr., E.A., Butler, J.C., Carman Jr, M.F., 1971. The lunar regolith as sampled by Apollo 11 and Apollo 12: Grain size analyses, modal analyses, and origins of particles. In: Proc. 2nd Lunar Sci. Conf., pp. 737–746.
Korotev, R.L., 1982. Comparative geochemistry of Apollo 16 surface soils and samples from cores 64002 and 60002 thru 60007. In: Proc. 13th Lunar Planet. Sci. Conf., pp. A269–A278.
Korotev, R.L., Gillis, J.J., 2001. A new look at the Apollo 11 regolith and KREEP. J. Geophys. Res. 106, 12339–12353.
Logan, L.M., Hunt, G.R., 1970. Emission spectra of particulate silicates under simulated lunar conditions. J. Geophy. Res. 75, 6539–6548.
Logan, L.M., Hunt, G.R., Salisbury, J.W., et al., 1973. Compositional implications of Christiansen frequency maximums for infrared remote sensing applications. J. Geophy. Res. 78, 4983–5003.
Lucey, P.G., Greenhagen, B.T., Song, E., et al., 2016. Space weathering effects in Diviner Radiometer measurements of the lunar Christiansen Feature: Characteristics and mitigation. Icarus doi:10.1016/j.icarus.20015.05.010, in press.
Lyon, R.J.P. (1964), Evaluation of infrared spectrophotometry for compositional analysis of lunar and planetary soils, part II, Rough and powdered surfaces, *NASA Rep. CR-100*, 264 pp.
Maturilli, A., Donaldson Hanna, K.L., Helbert, J., et al., 2013. A new standard for calibration of high temperature emissivity: Laboratory intercalibration at PEL of DLR and ALEC of Brown University. In: Proc. Lunar Planet. Sci. Conf., p. 1890.
Maturilli, A., Helbert, J., Witzke, A., et al., 2006. Emissivity measurements of analogue materials for the interpretation of data from PFS on Mars Express and MERTIS on Bepi-Colombo. *Planet. Space Sci.* 54, 1057–1064.
McKay, D.S., Heiken, G.H., Taylor, R.M., et al., 1972. Apollo 14 soils: Size distribution and particle types. In: Proc. 3rd Lunar Sci. Conf., pp. 983–995.
Morris, R.V., 1978. The surface exposure (maturity) of lunar soils: Some concepts and Is/FeO compilation. In: Proc. Lunar Sci. Conf., 9, pp. 2287–2297.
Morris, R.V., 1976. Surface exposure indices of lunar soils: A comparative FMR study. In: Proc. Lunar Sci. Conf., 7, pp. 315–335.
Murcray, F.H., 1965. The spectral dependence of lunar emissivity. *J. Geophys. Res.* 70, 4959–4962.
Nash, D.B., Salisbury, J.W., Conel, J.E., et al., 1993. Evaluation of infrared emission spectroscopy for mapping the Moon's surface composition from lunar orbit. J. Geophys. Res. 98 (E12), 23,535–23,552.
Nash, D.B., Salisbury, J.W., 1991. Infrared reflectance spectra (2.2–15 μm) of plagioclase feldspars. Geophys. Res. Let. 18, 1151–1154.
Noble, S.K., Pieters, C.M., Hiroi, T., et al., 2006. Using the modified Gaussian model to extract quantitative data from lunar soils. J. Geophy. Res. 111. doi:10.1029/2006JE002721.
Noble, S.K., Keller, L.P., Pieters, C.M., 2005. Evidence for space weathering in regolith breccias I: Lunar regolith breccias. Meteor. Planet. Sci. 40, 397–408.
Noble, S.K., Pieters, C.M., Taylor, L.A., et al., 2001. The optical properties of the finest fraction of lunar soil: Implications for space weathering. Meteor. Planet. Sci. 36, 31–42.
Paige, D.A., Foote, M.C., Greenhagen, B.T., 2010. The lunar reconnaissance orbiter Diviner lunar radiometer experiment. Space Sci. Rev. 150, 125–160. doi:10.1007/s11214-009-9529-2.
Paige, D.A., Seigler, M.A., Zhang, J., et al., 2010. Diviner Lunar Radiometer observations of cold traps in the Moon's south polar region. Science 330, 479–482. doi:10.1126/science.1187726.
Pieters, C.M., Shkuratov, Y., Kaydash, V.G., et al., 2006. Lunar soil characterization consortium analyses: Pyroxene and maturity estimates derived from Clementine image data. Icarus 184, 83–101. doi:10.1016/j.icarus.1006.04.013.
Pieters, C.M., Taylor, L.A., McKay, D.S., et al., 2000. Spectral characterization of lunar mare soils. In: Proc. Lunar Planet. Sci. Conf., 31, p. 1865.
Pieters, C.M., Fischer, E.M., Rode, O., et al., 1993. Optical effects of space weathering: The role of the finest fraction. J. Geophy. Res. 98, 20,817–20,824.
Ramsey, M.S., Christensen, P.R., 1998. Mineral abundance determination: Quantitative deconvolution of thermal emission spectra. J. Geophy. Res. 103, 577–596.
Rhodes, J.M., Rodgers, K.V., Shih, C., et al., 1974. The relationships between geology and soil chemistry at the Apollo 17 landing site. In: Proc. 5th Lunar Sci. Conf., pp. 1097–1117.
Rogers, A.D., Bandfield, J.L., Christensen, P.R., 2007. Global spectral classification of martian low-albedo regions with Mars Global Surveyor Thermal Emission Spectrometer (MGS-TES) data. J. Geophys. Res. 112. doi:10.1029/2006JE002726.
Rose, H.J., Baedecker, P.A., Berman, S., et al., 1975. Chemical composition of rocks and soils returned by the Apollo 15, 16, and 17 missions. In: Proc. 6th Lunar Sci. Conf., pp. 1363–1373.
Rose, H.J., Cuttitta, F., Berman, S., et al., 1974. Chemical composition of rocks and soils at Taurus–Littrow. In: Proc. 5th Lunar Sci. Conf., pp. 1119–1134.
Rose, H.J., Cuttitta, F., Annell, C.S., et al., 1972. Compositional data for twenty-one Fra Mauro lunar materials. In: Proc. 3rd Lunar Sci. Conf., pp. 1215–1229.
Ruff, S.W., Christensen, P.R., Barbera, P.W., et al., 1997. Quantitative thermal emission spectroscopy of minerals: A laboratory technique for measurement and calibration. J. Geophy. Res 102, 14899–14913.
Salisbury, J.W., Wald, A., 1992. The role of volume scattering in reducing spectral contrast of reststrahlen bands in spectra of powdered minerals. Icarus 96, 121–128.
Salisbury, J.W., Walter, L.S., 1989. Thermal infrared (2.5-13.5 microns) spectroscopic remote sensing of igneous rock types on particulate planetary surfaces. J. Geophy. Res. 94, 9192–9202.
Shirley, K.A., Glotch, T.D., 2015. First measurements from the planetary and Asteroid Regolith Spectroscopy Environment Chamber (PARSEC). In: Proc. 46th Lunar Planet. Sci. Conf., p. 2025.
Simon, S.B., Papike, J.J., Laul, J.C., 1981. The lunar regolith: Comparative studies of the Apollo and Luna sites. In: Proc. 12th Lunar Planet. Sci. Conf., pp. 371–388.
Song, E., Bandfield, J.L., Lucey, P.G., et al., 2013. Bulk mineralogy of lunar crater central peaks via thermal infrared spectra from the Diviner Lunar Radiometer: A study of the Moon's crustal composition at depth. J. Geophy. Res. 118. doi:10.1002/jgre.20065.
Taylor, G.J., Martel, L.M.V., Lucey, P.G., et al., 2012. Modal analyses of Apollo 16 soils by X-ray diffraction. In: Proc. 43rd Lunar Planet. Sci. Conf., p. 2316.
Taylor, L.A., Pieters, C., Patchen, A., et al., 2010. Mineralogical and chemical characterization of lunar highland soils: Insights into the space weathering of soils on airless bodies. J. Geophy. Res. 115. doi:10.1029/2009JE003427.
Taylor, L.A., Pieters, C.M., Keller, L.P., et al., 2001. Lunar mare soils: Space weathering and the major effects of surface-correlated nanophase Fe. *J. Geophy. Res.* 106, 27,985–27,999.
Thomas, I.R., Greenhagen, B.T., Bowles, N.E., et al., 2012. A new experimental setup for making thermal emission measurements in a simulated lunar environment. Rev. Sci. Instrum. 83, 124502. doi:10.1063/1.4769084.
Vasavada, A.R., Bandfield, J.L., Greenhagen, B.T., et al., 2012. Lunar equatorial surface temperatures and regolith properties from the Diviner Lunar Radiometer Experiment. J. Geophy. Res. 117. doi:10.1029/2011JE003987.
Vasavada, A.R., Paige, D.A., Wood, S.E., 1999. Near-surface temperatures on Mercury and the Moon and the stability of polar ice deposits. Icarus 141, 179–193.
Warren, T.J., Thomas, I.R., Bowles, N., 2014. The Oxford Space Environment Goniometer. In: Proc. Lunar Planet. Sci. Conf., 45, p. 1874.
Willis, J.P., Erlank, A.J., Gurney, J.J., et al., 1972. Major, minor, and trace element data for some Apollo 11, 12, 14 and 15 samples. In: Proc. 3rd Lunar Sci. Conf., pp. 1269–1273.
Wyatt, M.B., Hamilton, V.E., McSween Jr., H.Y., et al., 2001. Analysis of terrestrial and martian volcanic compositions using thermal emission spectroscopy: I. Determination of mineralogy, chemistry, and classification strategies. J. Geophy. Res. 106, 14711–14732.